

PALEOPROTEROZOIC DEFORMATION AND METAMORPHISM IN THE  
PEACOCK MOUNTAINS, NORTHWEST ARIZONA: IMPLICATIONS FOR  
PALEOPROTEROZOIC TECTONICS

By Mitchell Ryan Prante

A Thesis

Submitted in Partial Fulfillment  
of the Requirements for the Degree of  
Master of Science  
in Geology

Northern Arizona University

December 2009

Approved:

---

Ernest M. Duebendorfer, Ph.D., Chair

---

Thomas D. Hoisch, Ph.D.

---

Paul Umhoefer, Ph.D.

## ABSTRACT

### **Paleoproterozoic deformation and metamorphism in the Peacock Mountains, northwest Arizona: Implications for Paleoproterozoic tectonics**

Mitchell Ryan Prante

The Paleoproterozoic crust of southwest Laurentia has been divided into three provinces, the Mojave, Yavapai, and Mazatzal, based largely on Nd and Pb isotopic characteristics. The boundary between the Mojave and Yavapai crustal provinces has been described as a 75+ km-wide zone of mixed Pb isotopic signatures. The eastern margin of this zone is generally agreed to coincide with a sharp break in Pb isotopic character approximately coincident with the Crystal shear zone in the Upper Granite Gorge of the Grand Canyon. The location of the western margin is more controversial and the Peacock Mountains, northwestern Arizona, are located between two proposed locations for this margin. In the Lower Granite Gorge of the Grand Canyon, the Gneiss Canyon shear zone, commonly considered the western margin of the Mojave-Yavapai boundary zone, coincides with a transition from granulite facies metamorphism (to west) to amphibolites facies metamorphism (to east). An along-strike, southwestward projection of the Gneiss Canyon shear zone lies west of the Peacock Mountains and would continue between the Hualapai and Cerbat Mountains. This study used detailed geologic mapping, thermobarometry, and petrologic work in the Peacock Mountains to better understand the position of this boundary and to propose a tectonic setting for the boundary zone between the Mojave and Yavapai crustal provinces.

The Peacock Mountains contain evidence for two penetrative Paleoproterozoic deformational events. The first deformational event ( $D_1$ ) is characterized by a west- to

northeast-striking, steeply dipping foliation, and intrafolial, isoclinal folds. The second deformational event ( $D_2$ ) is characterized by a west- to west-northwest-trending, shallowly- to steeply-plunging lineation, and west- to northwest plunging, tight to open folds. These deformational events are thought to be correlative to previously identified and dated deformation events in western Arizona. The first of these events ( $D_1$ ) has been attributed to the collision of the Mojave and Yavapai crustal provinces, and has been dated at approximately 1740-1710 Ma. The second of these events is the Yavapai orogeny ( $D_2$ , 1700-1685 Ma) and has been attributed to the collision of the Mojave and Yavapai provinces onto previously accreted Paleoproterozoic terranes in the central Colorado Rocky Mountains.

Pressure and temperature conditions in the Peacock Mountains are anomalously low compared to other ranges in the Mojave province. Minimum pressure and temperature conditions of 4.5 kbars and  $\sim 600$  °C were determined using the GASP barometer and garnet-biotite thermometer and no evidence for partial melting of pelitic rocks was observed.

The association of continentally derived, quartz-rich metasedimentary rocks with mafic and intermediate metavolcanic rocks is most consistent with an extensional back-arc basin setting for the Peacock Mountains. Therefore, in the model presented in this study, the Mojave-Yavapai boundary zone formed as a result of repeated back-arc extension and tectonic switching.

## ACKNOWLEDGMENTS

I must acknowledge Ernest Duebendorfer for his endless help and support. His patient and humble reviews of manuscripts and grant applications has directly contributed to the completion of this thesis. In addition, he has become a close and invaluable friend. I want to thank my committee members, Dr. Tom Hoisch and Dr. Paul Umhoefer for their countless hours of assistance and advice. I would also like to thank Dr. Jim Wittke for assistance with the microprobe and scanning electron microscope.

I thank my fellow graduate students in the Department of Geology for hours of humor and distraction; with special thanks to Doug Portis for enumerable hours of assistance and discussion of thesis topics and details.

Financial support for this project was provided by the Geological Society of America, Four Corners Geological Society, and Tom and Rose Bedwell Earth Physics Award (Sigma Xi).

Finally, I must acknowledge my family, Robin Nagy, Mom, and Dad (Terri and Scot) for moral and financial support during this endeavor.

## Table of Contents

<b>List of Tables .....</b>	<b>viii</b>
<b>List of Figures.....</b>	<b>ix</b>
<b>Chapter 1 .....</b>	<b>1</b>
Introduction and Goals of This Study .....	1
GEOLOGIC SETTING .....	2
Mojave Province .....	2
Yavapai Province .....	4
Mojave-Yavapai Province Boundaries .....	4
Timing of Deformation .....	6
Proterozoic crustal growth and assembly in the southwestern US .....	9
<b>Chapter 2 .....</b>	<b>13</b>
<b>Description of Rock Units .....</b>	<b>13</b>
Metamorphic Rocks .....	14
Paleoproterozoic Metasedimentary Schist (Xms).....	14
Metamorphosed Plutonic and Volcanic Rocks .....	25
Paleoproterozoic Mafic Gneiss (Xmg) .....	25
Paleoproterozoic Undifferentiated Granite (Xgr) .....	29
Paleoproterozoic Megacrystic Granite (Xgrm).....	30
Unmetamorphosed Plutonic and Volcanic Rocks.....	32
Paleo-Mesoproterozoic Undifferentiated Granite (XYgr) .....	32
Diabase Dikes (green stipple) .....	35
Tertiary and Quaternary rocks .....	37

Tertiary Volcanic Rocks (Tv) .....	37
Quaternary Alluvium (Qal).....	38
<b>Chapter 3 .....</b>	<b>39</b>
<b>Structural Geology.....</b>	<b>39</b>
Regional Deformation.....	39
Deformation in the Southern Peacock Mountains .....	39
Introduction.....	39
Evidence for Polyphase Deformation .....	40
Paleoproterozoic Deformation .....	41
S <sub>1</sub> Foliation.....	41
F <sub>1</sub> folds .....	44
F <sub>2</sub> folds .....	46
L <sub>2</sub> lineation.....	48
Interpretation and Conclusions .....	54
<b>Chapter 4 .....</b>	<b>58</b>
<b>Conditions of Metamorphism .....</b>	<b>58</b>
Introduction.....	58
Metasedimentary schist.....	58
Garnet.....	60
Sillimanite .....	60
Muscovite.....	60
Biotite.....	61
Interpretation.....	61

Thermobarometry .....	64
Introduction.....	64
Methods and Results.....	64
Conclusions and regional significance.....	68
<b>Chapter 5 .....</b>	<b>69</b>
<b>Tectonic Implications .....</b>	<b>69</b>
Introduction.....	69
Hualapai Mountains .....	71
Cerbat Mountains.....	73
Cottonwood Cliffs.....	74
Poachie Range.....	75
Central Arizona.....	76
Tectonic Setting of the Peacock Mountains.....	76
Tectonic Model .....	78
<b>Chapter 6 .....</b>	<b>82</b>
<b>Conclusions.....</b>	<b>82</b>
Conclusions.....	82
<b>References.....</b>	<b>84</b>
<b>Appendix A.....</b>	<b>94</b>
<b>Appendix B .....</b>	<b>98</b>
<b>Biographical Information.....</b>	<b>101</b>

## List of Tables

<b>Table 1:</b> General Characteristics of Provinces and Transition Zone.....	8
<b>Table 2:</b> Description of Map Units.....	13
<b>Table 3:</b> General Characteristics of Local and Regional Deformation.....	40
<b>Table 4:</b> Summary of geochronologic data.....	70

## List of Figures

<b>Figure 1-1:</b> Map of southwestern United States with Proterozoic crustal provinces and provincial boundaries.....	3
<b>Figure 1-2:</b> Simplified map of northwestern Arizona with generalized distribution of Pb isotopic data in Delta Jerome units.....	5
<b>Figure 1-3:</b> Alternative models for the formation of the Mojave-Yavapai boundary zone.....	11
<b>Figure 1-4:</b> Banda Sea model for crustal growth in the southwest United States.....	12
<b>Figure 2-1:</b> Field photograph of metasedimentary schist.....	16
<b>Figure 2-2:</b> Photomicrographs of psammitic schist.....	19
<b>Figure 2-3:</b> Photomicrographs of pelitic schist.....	21
<b>Figure 2-4:</b> Field photograph and photomicrograph of pelitic schist.....	22
<b>Figure 2-5:</b> Photomicrographs of ultramafic rocks.....	24
<b>Figure 2-6:</b> Field photograph of mafic gneiss.....	27
<b>Figure 2-7:</b> Photomicrographs of mafic gneiss.....	28
<b>Figure 2-8:</b> Field photograph of Paleoproterozoic megacrystic granite.....	31
<b>Figure 2-9:</b> Field photograph and photomicrograph of Paleo-Mesoproterozoic undifferentiated granite.....	34
<b>Figure 2-10:</b> Photomicrograph of diabase dike.....	36
<b>Figure 3-1:</b> Stereonet of structural data collected in the Peacock Mountains.....	42
<b>Figure 3-2:</b> Stereonet of poles to $S_1$ foliation from the Peacock Mountains .....	43
<b>Figure 3-3:</b> Field photograph of $F_1$ folds.....	45
<b>Figure 3-4:</b> Field photograph of $F_2$ folds.....	47

<b>Figure 3-5:</b> Stereonet of lineation data.....	51
<b>Figure 3-6:</b> Strike vs. rake plot of lineation data.....	52
<b>Figure 3-7:</b> Schematic line drawing of D <sub>2</sub> folds and lineation.....	53
<b>Figure 3-8:</b> General foliation trajectory map of Paleoproterozoic foliation.....	57
<b>Figure 4-1:</b> Map with pressure and temperature conditions of Paleoproterozoic ranges in northwest Arizona.....	59
<b>Figure 4-2:</b> Petrogenetic grid.....	63
<b>Figure 4-3:</b> Garnet-biotite and GASP plot from Peacock Mountains.....	66
<b>Figure 4-4:</b> Error envelope associated with GASP calculation.....	67
<b>Figure 5-1:</b> Simplified geologic map of Paleoproterozoic rocks in NW Arizona.....	71
<b>Figure 5-2:</b> Preliminary tectonic model for pre-D <sub>1</sub> rifting and D <sub>1</sub> collision.....	81

## **List of Plates**

**Plate 1:** Geologic Map of the Peacock Mountains

## Chapter 1

### Introduction and Goals of This Study

Proterozoic rocks of the southwest United States provide insight into crustal processes at all scales. Exposures of Precambrian rocks extending from southern Wyoming, United States, to Sonora, Mexico, have been associated with the successive accretion of island arcs, associated marginal basins, and microcontinents (Condie, 1982; Karlstrom and Bowring, 1991; Whitmeyer and Karlstrom, 2007).

The Proterozoic crust of southwest Laurentia has been divided into three crustal provinces based on isotopic and geochronologic data, the Mojave, Yavapai, and Mazatzal (Bennett and DePaolo, 1987; Chamberlin and Bowring, 1990). The Peacock Mountains are located between two proposed locations for the western margin of the boundary zone between the Mojave and Yavapai provinces (Fig. 1-1). The nature and location of boundaries between crustal blocks is pivotal to understanding the history of crustal growth in the southwest United States.

In this thesis, I propose a model for the original tectonic setting for the Peacock Mountains and the early stages of deformation related to juxtaposition of the Mojave and Yavapai provinces. Specific goals of this study are to: 1) determine the pressure and temperature history of the Peacock Mountains to test the prevailing hypothesis that the northeast-striking Gneiss Canyon shear zone is the western margin of the Mojave-Yavapai boundary zone, (2) evaluate the significance of anomalously oriented deformational fabrics to place the range into a regional structural context, and (3) propose a possible tectonic setting for large volumes of quartz-rich sedimentary rocks and

associated mafic volcanic and volcanoclastic rocks in the central and southern Peacock Mountains.

## **GEOLOGIC SETTING**

### **Mojave Province**

The Mojave province consists of Paleoproterozoic amphibolite to granulite facies migmatitic quartzofeldspathic gneiss, amphibolite, pelitic and psammitic schist, and ultramafic rocks. These rocks have been intruded by a suite of granitoids of variable composition (Wooden and Miller, 1990; Miller and Wooden, 1992; Anderson et al. 1993).

Based on Pb and Nd isotopic compositions, the Mojave province is regarded as having evolved (continental) crust. The Mojave province has Nd model ages between 2.3 and 2.0 Ga; these model ages are from rocks with crystallization ages of 1.76 Ga or younger (Bennett and DePaolo, 1987). The Nd model ages have been interpreted to represent an average of the crustal components of the Mojave province, suggesting involvement of older crust (Wooden and Dewitt, 1991). The Mojave province has rocks with crystallization ages of 1.78-1.68 Ga, but the high initial ratios of radiogenic lead were interpreted by Wooden et al. (1988) to indicate some component of older crust. The presence of some component of older crust is confirmed by detrital zircons in metasedimentary rocks and inherited zircons that range from 2.8 to 1.8 Ga in granitoids (Wooden et al., 1988; 1994; Wooden and Miller, 1990; Duebendorfer et al., 2001). See Table 1 for general characteristics of Mojave province.

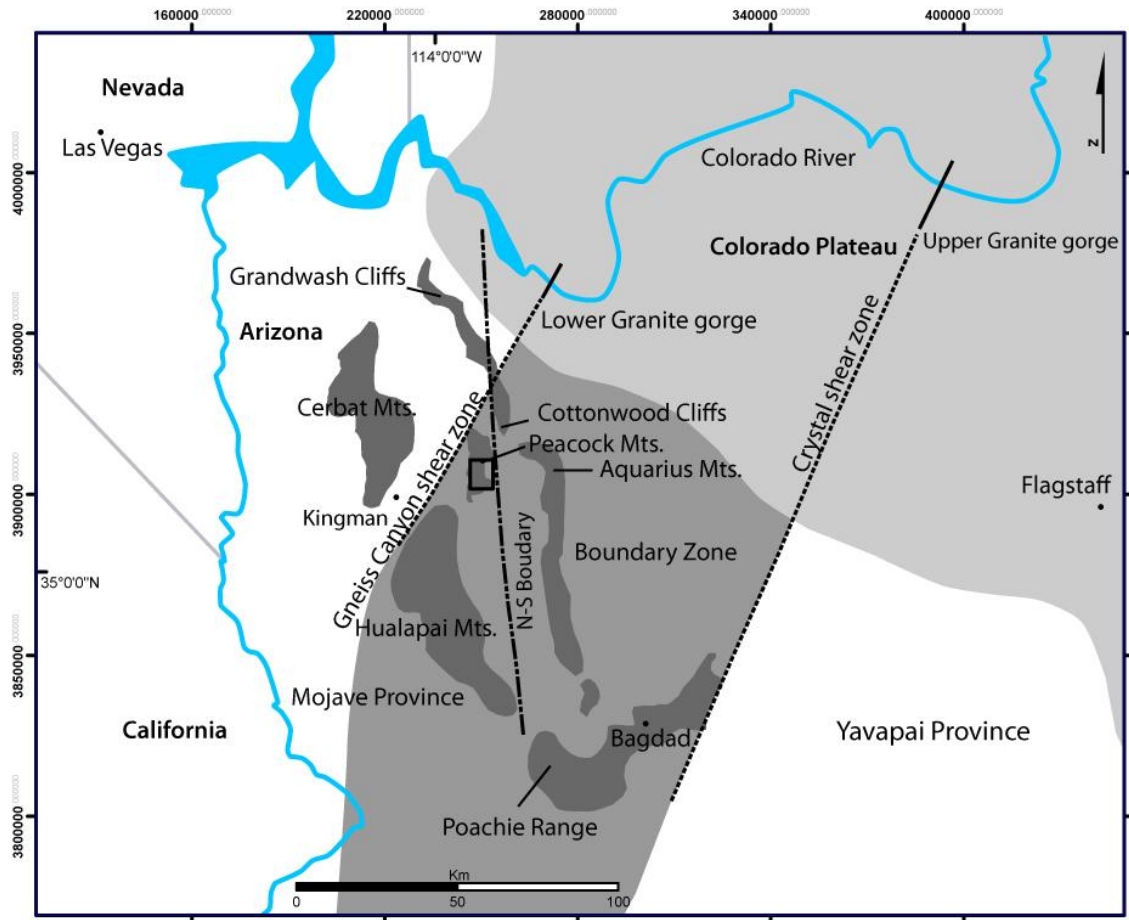


Figure 1-1: Field area (box), located between Gneiss Canyon shear zone, which was proposed as the western margin of the isotopically complex boundary zone (intermediate gray) (after Wooden and DeWitt (1991)) by Albin and Karlstrom (1991), and a N-S boundary, proposed by Duebendorfer et al. (2006). NAD 27, UTM Zone 11N.

## **Yavapai Province**

The Yavapai province consists of greenschist to amphibolite facies pelitic and psammitic schist, felsic to mafic volcanic and intermediate plutonic rocks, and volcanogenic metasedimentary rocks (Anderson et al., 1971; Anderson and Silver, 1976; Karlstrom and Bowring, 1988; Anderson, 1989). Rocks in the Yavapai province have Nd model ages from 1.70 to 1.85 Ga (Bennett and DePaolo, 1987). These dates are close to the crystallization ages of approximately 1.75-1.68 Ga; therefore, the Yavapai province is considered to have juvenile (oceanic island-arc) crust (Fig. 1-2). Based upon rock types and Nd and Pb isotopic compositions, the Yavapai province was likely produced from a depleted mantle reservoir alone and pre-existing crust was not involved (Wooden and DeWitt, 1991). See Table 1 for general characteristics of Yavapai province.

## **Mojave-Yavapai Province Boundaries**

Wooden and DeWitt used a normalization technique to emphasize regional differences in  $^{207}\text{Pb}/^{204}\text{Pb}$  by comparing them to a galena standard at Jerome, Arizona. The normalized value, delta Jerome, is typically  $< 2$  for rocks in the Yavapai province and  $> 6$  for Mojave rocks. Wooden and DeWitt (1991) proposed the presence of a 75 km-wide north-northeast-trending boundary zone between the Mojave and Yavapai provinces that has Pb isotopic signatures intermediate between the two provinces (Fig. 1-2). The eastern margin of the boundary zone is located east of Bagdad, Arizona (Wooden and DeWitt, 1991), and coincides with the Crystal shear zone (Fig. 1-1) of the Upper Granite Gorge in Grand Canyon (Hawkins et al., 1996; Ilg et al., 1996). The location of this margin is based on a sharp change in Pb isotopic character and is widely agreed upon.

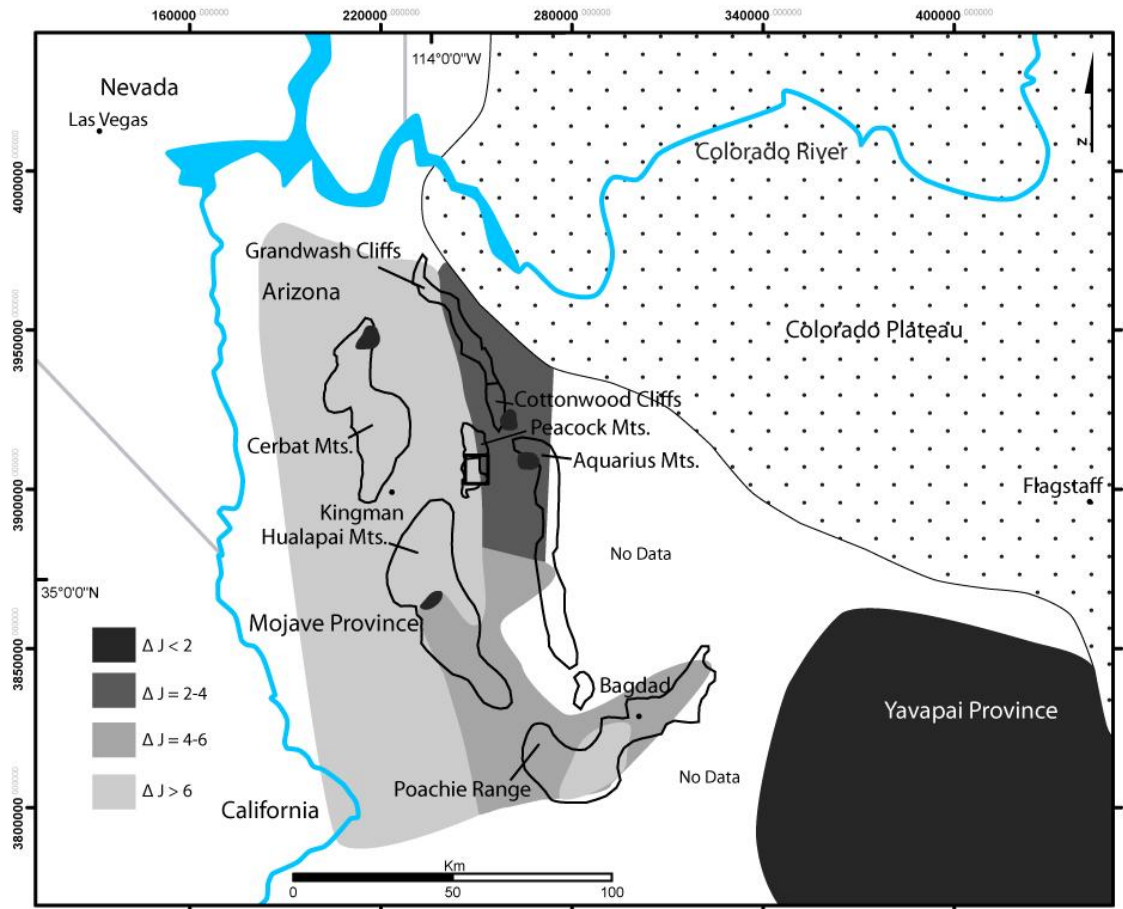


Figure 1-2: Simplified map of northwestern Arizona with generalized distribution of Pb isotopic data in Delta Jerome units. Delta Jerome unit is used as defined by Wooden and DeWitt (1991), Field area (box). NAD 27, UTM Zone 11N. Modified from Duebendorfer et al. (2006).

The location and nature of the western margin of the boundary zone is more enigmatic. Albin and Karlstrom (1991) suggested that the western margin of the boundary zone is an along-strike continuation of the Gneiss Canyon shear zone located in the Lower Granite Gorge of Grand Canyon, and that it projects directly northwest of the Peacock Mountains (Fig. 1-1). In the Grand Canyon, the Gneiss Canyon shear zone separates granulite facies rocks to the west from amphibolite facies rocks to the east (Robinson, 1994). A more recent hypothesis proposes an approximately north-south-trending line east of the Peacock Mountains as the western margin of the boundary zone. This margin is based on sharp discontinuities in Pb isotopes, geochemical, and geophysical signatures, as well as an abrupt change in metamorphic grade across that line (Duebendorfer et al., 2006). See Table 1 for general characteristics of Mojave-Yavapai boundary zone.

### **Timing of Deformation**

Two deformational events have been documented in both the Mojave and Yavapai crustal provinces. The first event, D<sub>1</sub> (1740-1710 Ma; Karlstrom and Bowring, 1988; Hawkins et al., 1996; Duebendorfer et al., 2001), is characterized by recumbent folds and a northwest-striking, gently northeast-dipping foliation. The second event, D<sub>2</sub> (1700-1685 Ma), is characterized by a subvertical, northeast-striking foliation. D<sub>1</sub> has been interpreted as recording the juxtaposition of the Mojave and Yavapai provinces (Duebendorfer et al. 2001). D<sub>2</sub> has been interpreted to represent the accretion of the Mojave and Yavapai provinces to previously accreted Paleoproterozoic terranes in the

central Colorado Rocky Mountains. It is important to mention that the history described above is not generally agreed upon. Karlstrom and Bowring (1988), Bowring and Karlstrom (1990), and Whitmeyer and Karlstrom (2007), view the  $D_1$  and  $D_2$  as representing a single protracted event.

Table 1. General Characteristics of Provinces and Transition Zone			
Feature	Mojave Province	Boundary Zone	Yavapai Province
<b>Age of magmatism</b>			
<b>Paleoproterozoic magmatism</b>			
Granitoids and volcanic rocks	1809-1635 Ma	1740-1620 Ma	1751-1625 Ma
<b>Mesoproterozoic magmatism</b>			
Granitoids	1430-1335 Ma	1411-1400 Ma	1480-1400Ma
Plutonic and volcanic rocks	1220-1069 Ma	1100 Ma	NA
<u>Plutonic rock type</u>	Monzogranite, syenogranite, granodiorite, diorite	Granodiorite, quartz monzonite, granite	Quartz diorite, tonalite, granite, granodiorite
<b>Deformation</b>			
Orogeny	Ivanpah orogeny (1.7 Ga)	Ivanpah-Yavapai orogeny	Ivanpah-Yavapai orogeny
Style	D <sub>1</sub> and D <sub>2</sub>	D <sub>1</sub> and D <sub>2</sub>	D <sub>1</sub> and D <sub>2</sub>
Granitoid formation	Pre-, Syn-, Postorogenic granites	Pre-, Syn-, Postorogenic granites	Pre-, Syn-, Postorogenic granites
<u>Age of detrital zircons in metasedimentary rocks</u>	2.8-1.8 Ga	NA	1.75-1.71 Ga
<u>Metamorphic grade</u>	High-amphibolite to granulite	Greenschist to low- to medium-amphibolite	Greenschist to low- to medium-amphibolite
<b>Geochemistry of Paleoproterozoic granitoids</b>			
<b>Major element</b>			
Geochemical series	High- to ultra-K calc-alkaline	High-K calc-alkaline	Calc-alkaline
Fe/Mg	High	High	Low
K <sub>2</sub> O in pre-, syn- orogenic granites	Very high (> 5.0 wt. %)	High	Low
<b>Trace Element and REE</b>			
Rb, Ba, Y, REE	Very enriched	Enriched	Depleted
Nd-Y discrimination plot	“Within plate” granites	“Within plate” and “volcanic arc” granites	“Volcanic arc” granites
<b>Radiogenic isotopes of Paleoproterozoic granitoids</b>			
<b>Pb isotopes</b>			
U/Pb	Low	High	High
Th/U	High (>4)	Average (~ 4)	Low (~ 2)
Th/Pb	High	Average	Low
<b>Nd isotopes</b>			
Nd model ages	2.3-2.0 Ga	Highly variable b/t Mojave and Yavapai	1.85-1.60 Ga 1.95-1.85 Ga in Grand Canyon

(modified after Iriondo et al., 2004)

## **Proterozoic crustal growth and assembly in the southwestern US**

Models for Proterozoic crustal growth and assembly in the southwestern United States must account for: (1) juxtaposition of tectonic blocks of variable ages across major shear zones, (2) multiple phases of deformation in Paleoproterozoic crustal provinces, (3) the juxtaposition of evolved (continental) crust (Mojave province) with juvenile (oceanic) crust (Yavapai province). In an early model, Condie (1982) proposed successive accretion of bimodal volcanic rocks and related siliciclastic assemblages to the southern margin of the Archean Wyoming craton in association with marginal basin closures. Karlstrom and Bowring (1988, 1993) suggested accretion of juvenile arcs as the principal mode of crustal growth. The latter view has been challenged by Hill and Bickford (2001) and Bickford and Hill (2007) who suggest that successive accretion of island arcs may be an oversimplification. Bickford and Hill (2007) proposed that bimodal igneous sequences and Pb, Nd, and Hf isotopic data that indicate the presence of 1800 Ma and older crust represents intracontinental rifting. In the Bickford and Hill (2007) model, magmatic additions to the crust via a rifting mechanism resulted in volumetrically significant additions of new crust. Duebendorfer et al. (2001) proposed that the Mojave and Yavapai crustal provinces were sutured together prior to being juxtaposed onto the Wyoming province, a departure from progressive southward crustal growth models (e.g., Condie, 1982). This hypothesis is supported by Coleman et al. (2000) who proposed that the Mojave and Yavapai provinces share a common history sometime after 1780 Ma based on detrital zircon provenance. Duebendorfer et al. (2006) proposed pre-collision rifting at the eastern margin of the Mojave province to explain the isotopically mixed and juvenile-type crust within the boundary zone (Fig. 1-3). In this model, rift basins are

envisioned as being floored by juvenile oceanic crust. On a more regional scale, Jessup et al. (2006) and Whitmeyer and Karlstrom (2007) suggested that the southwest Pacific (Banda Sea) is a modern analogue for the Paleoproterozoic orogen in the western United States. This model involves a complex system of island arcs, rift basins, subduction zones, and fragments of continental crust. This model accounts for disparate ages of volcanogenic sequences (interpreted as representing island arcs), multiple phases of deformation, and presence of older continental material (Fig. 1-4) (Jessup et al., 2006).

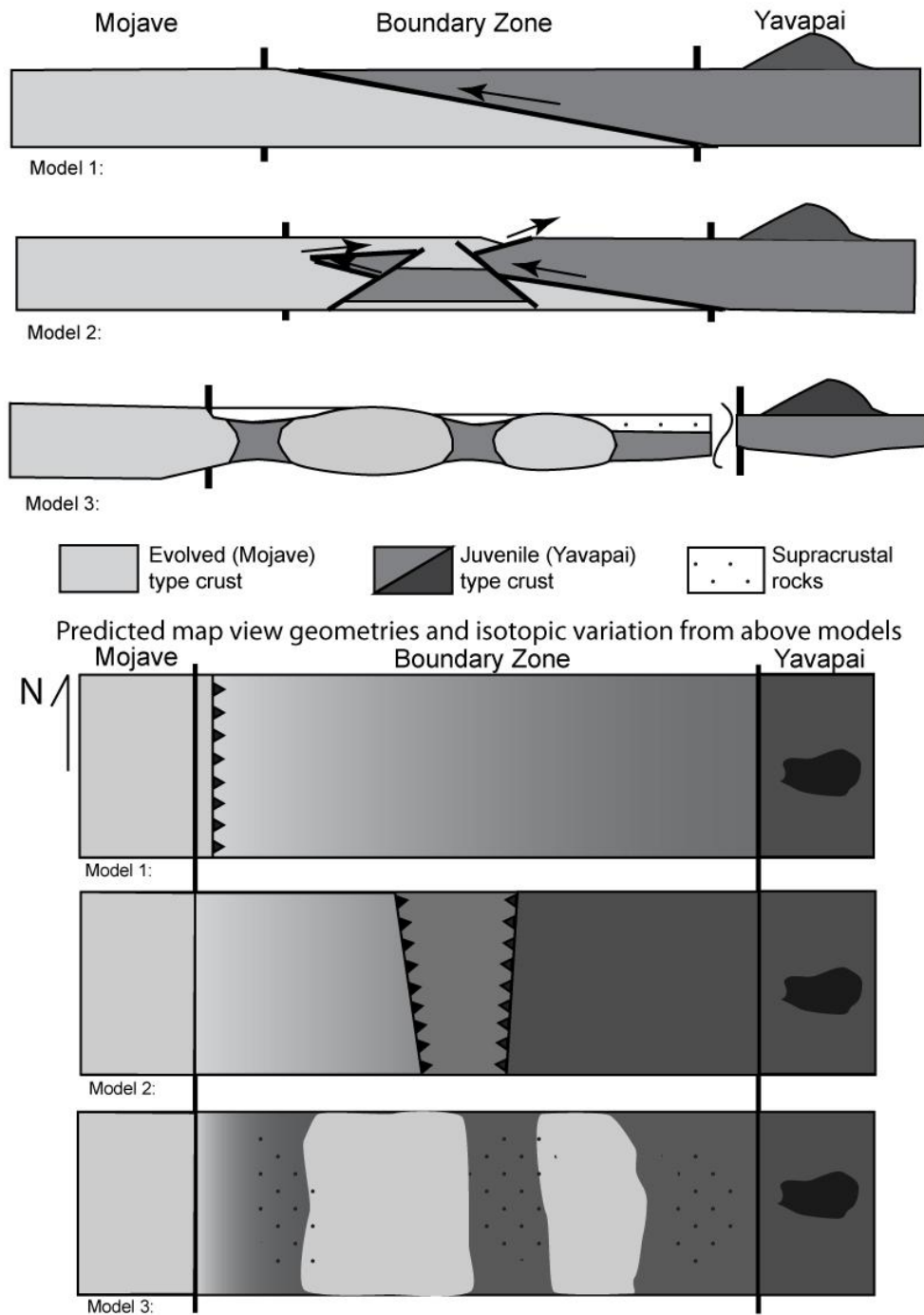


Figure 1-3: Alternative models for the formation of the isotopically complex boundary zone between the Mojave and Yavapai crustal provinces. Model 1: Tectonic juxtaposition along a discrete structure, Model 2: Schematic tectonic juxtaposition with crustal scale wedging and imbrication, Model 3: Pre-juxtaposition rifting of Mojave province, producing rift basins (stippled). Modified from Duebendorfer et al. (2006).

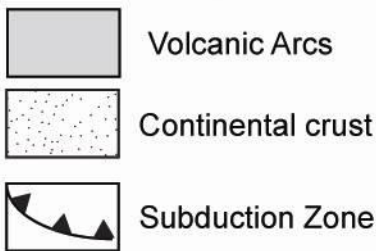
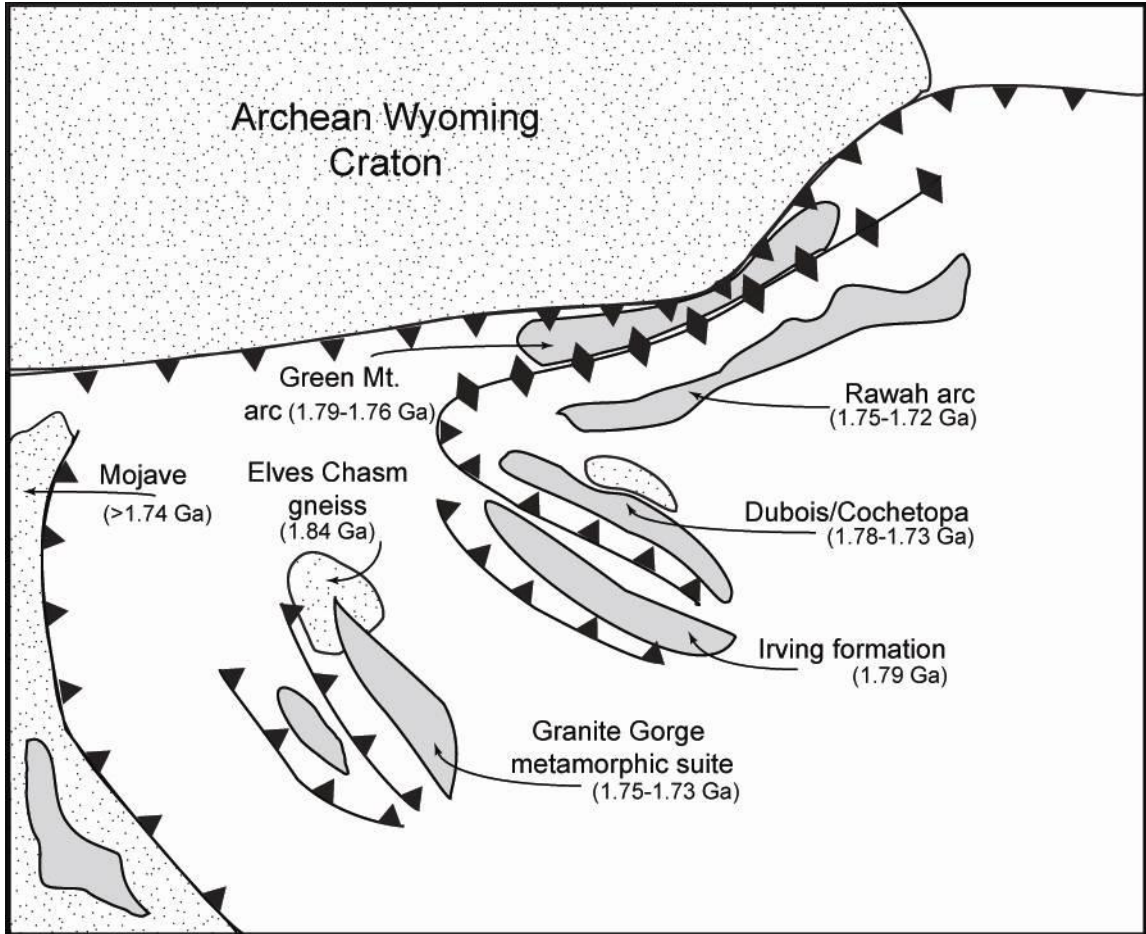


Figure 1-4: Banda Sea model for Paleoproterozoic crustal assembly in the southwest United States. This model is similar to the current configuration of the Banda Sea north of Australia (Hamilton, 1979). This hypothetical geometry illustrates the possibility of complex interactions between NW- and NE-striking subduction zones ca. 1.75 Ga. This model has been used to explain the formation of fabrics in the middle crust ca. 1.73-1.70 Ga in the Yavapai province. Modified from Jessup et al. (2005).

## Chapter 2

### Description of Rock Units

The map units in the southern Peacock Mountains consist of Paleoproterozoic metasedimentary rocks, mafic gneiss, deformed plutonic rocks, undeformed granite, megacrystic granite, Mesoproterozoic diabase dikes, and Tertiary volcanic rocks. Rock units are described in order from oldest to youngest, with relative ages established by cross-cutting relations. The following descriptions are based on both mesoscopic and microscopic observations and are followed by interpretations regarding possible origin of the unit. See Table 2 for general description and interpretation of map units. For a description of specific samples in thin section and list of phases present see Appendix A.

Map Unit	Description	Interpretation
Quaternary Alluvium (Qal)	Poorly sorted, unconsolidated sediment with clasts that range in size from silt to boulder.	
Tertiary Volcanic Rocks (Tv)	Undeformed basalt and andesite.	
Diabase Dikes (green stipple)	Undeformed medium- to coarse-grained mafic dikes.	Post-tectonic, 1.1 Ga dikes.
Paleo-Mesoproterozoic Undifferentiated Granite (X-Ygr)	Undeformed, medium- to coarse-grained granitic rocks.	Post-tectonic granite
Paleoproterozoic Megacrystic Granite (Xgrm)	Poorly foliated, medium- to coarse-grained granite containing cm-scale K-feldspar phenocrysts.	Pre- to syn- tectonic granitic rocks.
Paleoproterozoic Undifferentiated Granite (Xgr)	Foliated, locally lineated, medium- to coarse-grained granitic rocks.	Pre- to syn- tectonic granitic rocks.
Paleoproterozoic Mafic gneiss (Xmg)	Fine- to coarse-grained, strongly foliated and locally lineated mafic rocks. Locally contains gneissic foliation.	Interpreted to represent both mafic intrusions or flows and volcanogenic sediments
Paleoproterozoic Metasedimentary Schist (Xms)	Consists of psammitic schist, pelitic schist and minor mafic gneiss, and pods and lenses of ultramafic rocks. Unit is strongly foliated, locally lineated, and medium to coarse grained.	Interpreted to represent metamorphosed compositionally immature sandstone, shale and siltstone. May be consistent with a back-arc basin depositional environment.

## **Metamorphic Rocks**

### **Paleoproterozoic Metasedimentary Schist (Xms)**

The Paleoproterozoic metasedimentary schist unit consists of psammitic schist, pelitic schist (noted with stipple pattern on Plate 1), minor mafic gneiss, and ultramafic rocks. The metasedimentary schist is exposed in the central part of the map area (Plate 1). The unit is strongly foliated, locally lineated, and medium to coarse grained. Metasedimentary rocks are interleaved to such an extent that it was not possible to map them as separate units at the map scale of 1:12,000. Similarly, some of the mafic gneiss and ultramafic rocks occur as small pods or dikes which are too small to be resolved at the scale of the map. The metasedimentary schist has been intruded by several units including Paleoproterozoic undifferentiated granite (Xgr), Paleoproterozoic megacrystic granite (Xgrm), and Paleo-Mesoproterozoic undifferentiated granite (XYgr). The metasedimentary schist may have been depositionally interlayered with the mafic gneiss unit (Xmg), however, due to strong transposition in the map area, this remains conjectural

## **Psammitic Schist**

### **Macroscopic Description and Field Relations**

Psammitic schist in the southern Peacock Mountains is gray, medium to coarse grained, strongly foliated, and locally lineated. Psammitic schist occurs as layers approximately 50 cm to 10's m thick, and is the most voluminous rock type in the metasedimentary rock unit. The psammitic schist generally forms steep slopes and high ridges. The psammitic schist forms sharp contacts with the pelitic schist and mafic gneiss (Fig. 2-1).

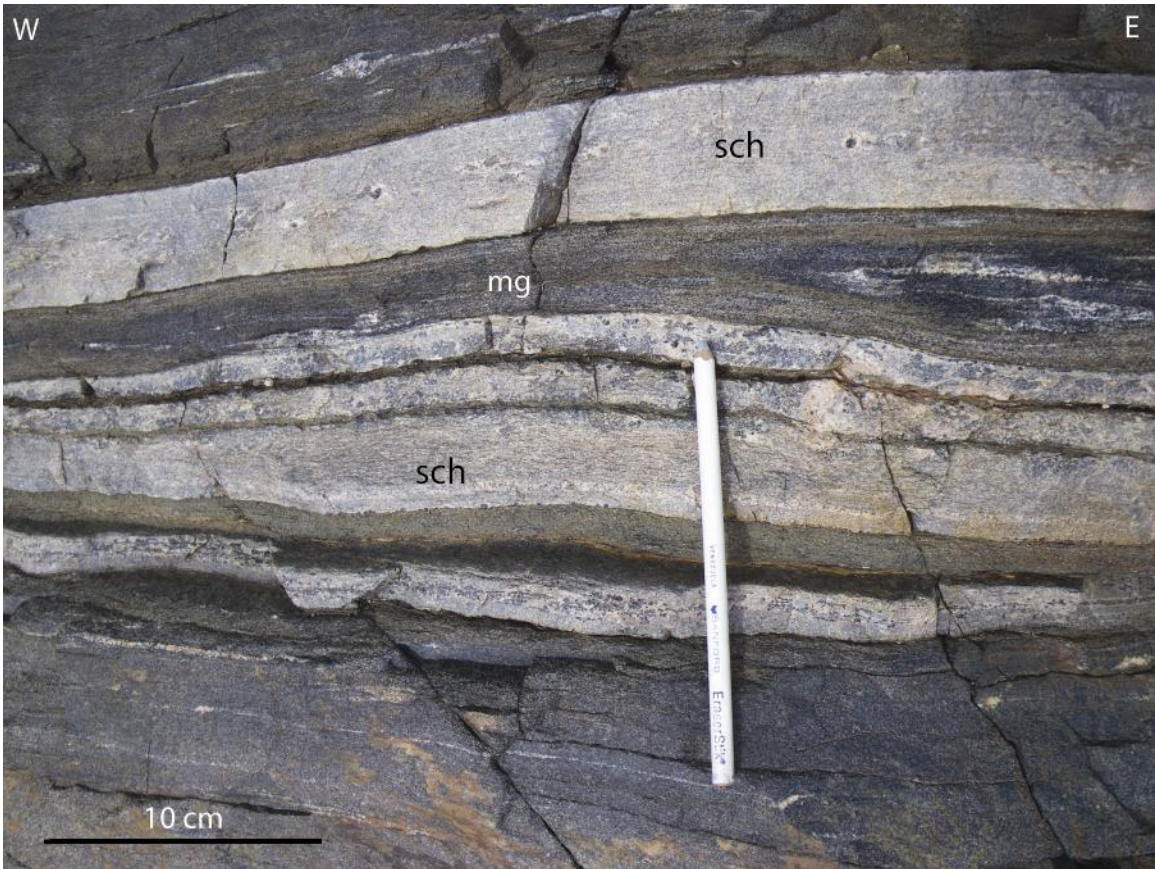


Figure 2-1: Field photograph of metasedimentary schist. Looking at a horizontal face, down dip. Pencil points to the north. 2-10 cm thick layering of psammitic schist (sch) and mafic gneiss (mg).

## **Petrology**

Psammitic schist is characterized by the mineral assemblage quartz + plagioclase + K-feldspar + biotite ± garnet ± hornblende ± muscovite ± sericite. Muscovite and sericite have been interpreted to represent retrograde phases based on the pseudomorphous morphology of these phases (Fig. 2-2). The quartz commonly has undulose extinction, subgrains, and rounded grain boundaries with tri-partate intersections at approximately 120° (Fig. 2-2). Some samples contain recrystallized quartz ribbons. These observations are interpreted to represent dynamic recrystallization of the quartz grains. The biotite in the psammitic schist is euhedral to subhedral and aligned with the long axis parallel to the foliation and lineation (Fig. 2-2). Plagioclase and K-feldspar grains are typically subhedral to anhedral, corroded, and have sericite alteration (Fig. 2-2). Hornblende grains in the psammitic schist are commonly porphyroblastic, poikiloblastic, and anhedral (Fig. 2-2). Garnet grains in the psammitic schist are porphyroblastic, poikiloblastic, and subhedral.

## **Interpretation**

The psammitic schist is interpreted to represent metamorphosed compositionally immature sandstone. However, due to high metamorphic grade no sedimentary structures were preserved to aid in interpretation of the depositional environment; therefore features such as composition and associated rocks have been used to interpret possible depositional environments. The presence of abundant feldspars suggests relatively short transport distance. Biotite and hornblende likely represent an original clay component of the sediment. The specific tectonic setting of the psammitic schist remains enigmatic; however, the presence of feldspar suggests possible proximity to a plutonic and/or

volcanic source area possibly with deposition in an intra- or back-arc basin (Marsaglia, 1995).

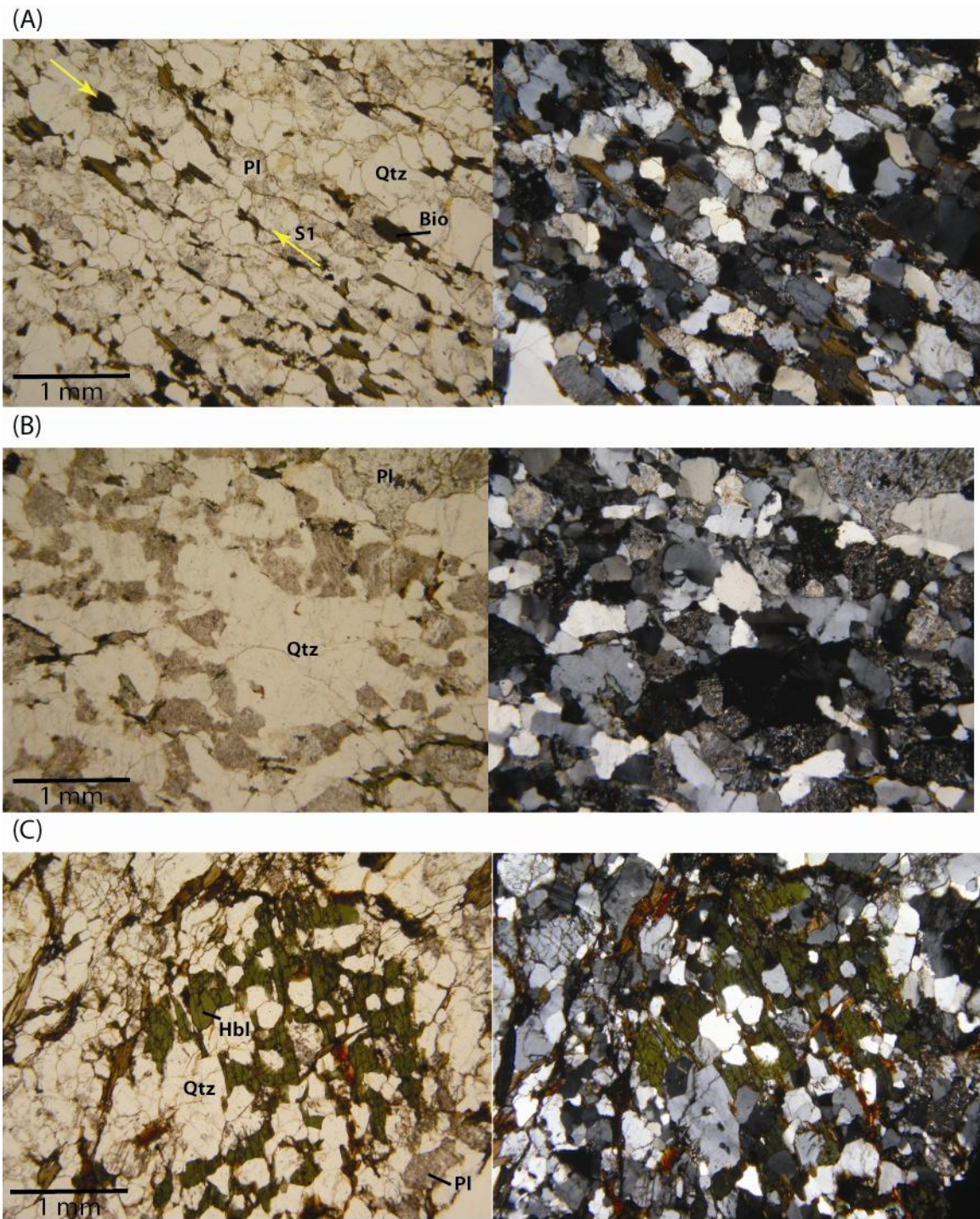


Figure 2-2: Photomicrographs of psammitic schist, ppl left, xpl right. (A) MP 5/26/08-6, biotite (Bio) and elongate quartz (Qtz) grains are aligned parallel to S1 foliation (yellow arrows). (B) MP 5/25/08-1, coarse-grained psammitic schist, plagioclase (Pl) contains sericite alteration. (C) MP 1/6/09-2, psammitic schist with anhedral and poikiloblastic hornblende (Hbl) porphyroblasts.

## **Pelitic Schist (stipple pattern)**

### **Macroscopic Description and Field Relations**

Pelitic schist in the Peacock Mountains is gray, medium to coarse grained, porphyroblastic, and moderately to strongly foliated. The pelitic schist occurs as layers and lenses between 50 cm to 10 m thick and is usually in sharp contact with psammitic schist.

### **Petrology**

Pelitic schist is characterized by the mineral assemblage quartz + K-feldspar + garnet + sillimanite + biotite + muscovite  $\pm$  plagioclase  $\pm$  spinel. Muscovite is interpreted as both a retrograde and a prograde phase, because it occurs as both euhedral grains aligned with the foliation (prograde) and as pseudomorphs after sillimanite (retrograde) (Fig. 2-3A). Garnet porphyroblasts are randomly oriented and locally rimmed by felsic halos of quartz, sillimanite, and muscovite (Fig. 2-3B, 2-4). Quartz is subhedral to anhedral and commonly has grain boundary intersections of 120°. Plagioclase is uncommon, anhedral, fine grained and contains sericite alteration (Fig. 2-3A). Sillimanite is fibrous, fine to medium grained, commonly rims garnet, and is typically present as inclusions in quartz. K-feldspar is subhedral and fine to medium grained.

### **Interpretation**

The pelitic schist is interpreted to represent metamorphosed shale and siltstone. This interpretation is based on the mineral assemblage described above. The mineral assemblages observed imply that the pelites have reached upper-amphibolite facies metamorphic conditions (see Chapter 4).

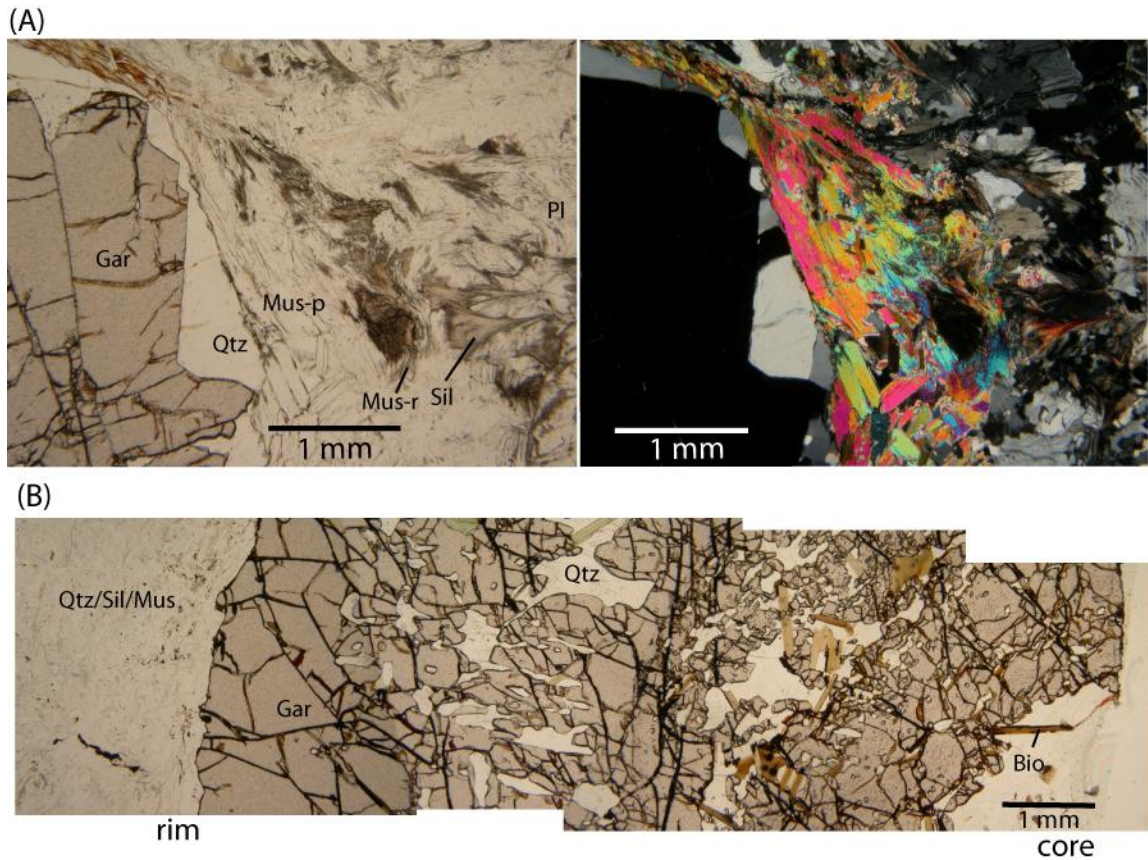


Figure 2-3: Photomicrographs of pelitic schist. (A) MP 5/14/08-1, ppl left, xpl right, retrograde muscovite (Mus-r) after sillimanite, possible prograde muscovite (Mus-p), and fibrous sillimanite (Sil). (B) MP 5/14/08-2, photomontage of garnet porphyroblast with quartz (Qtz) and biotite (Bio) inclusions. Garnet (Gar) porphyroblast is rimmed by quartz, sillimanite, and muscovite.

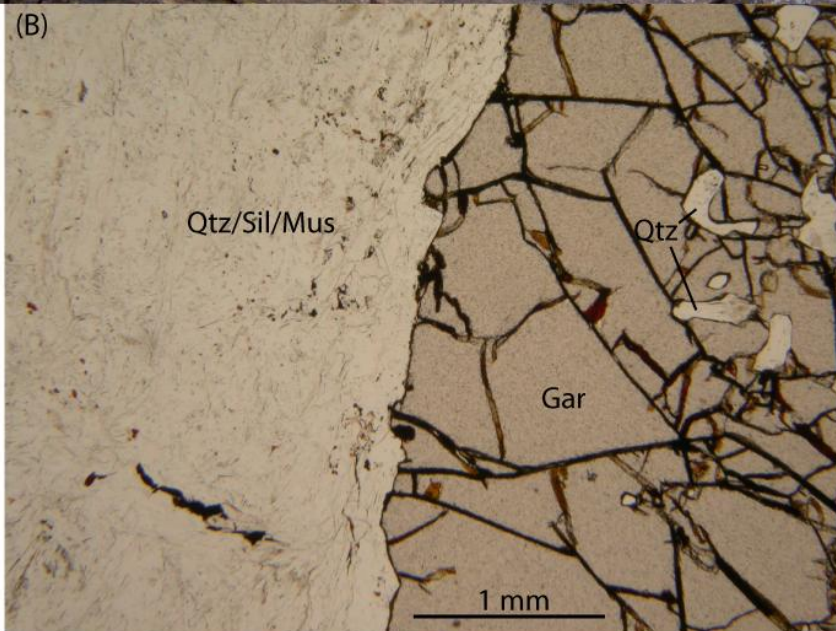
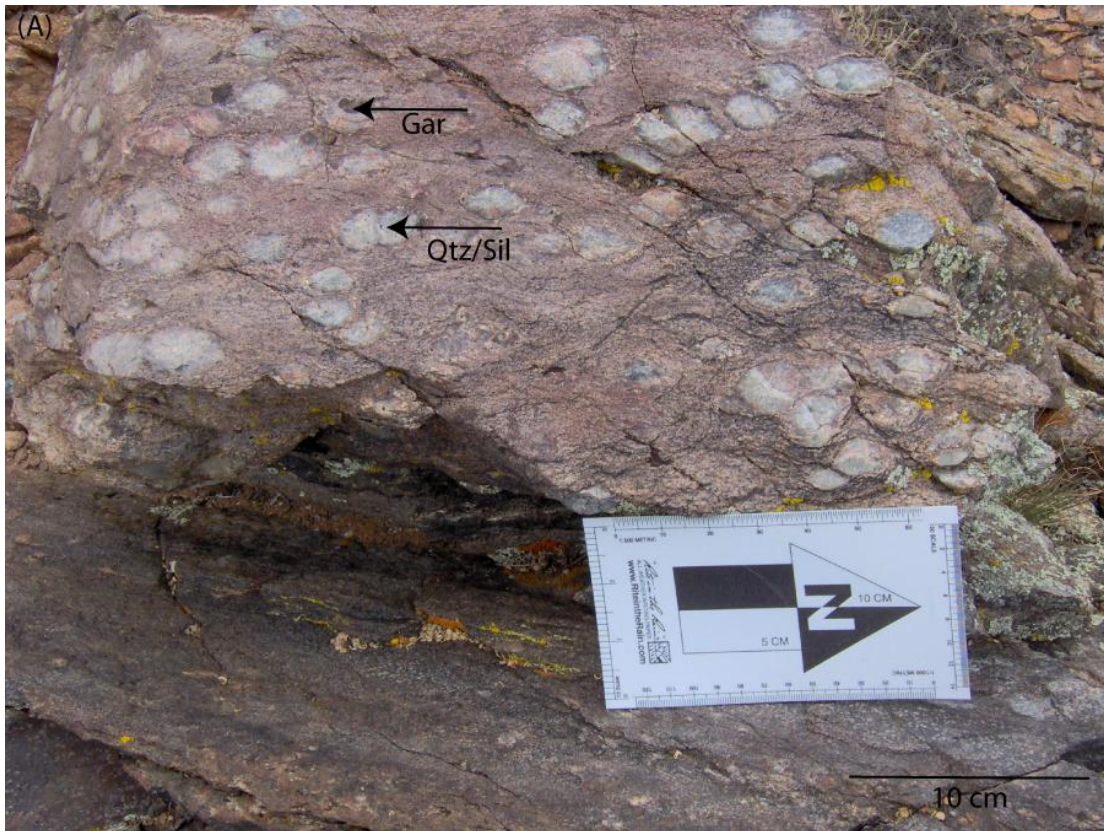


Figure 2-4: (A) Field photograph of pelitic schist, facing west at vertical outcrop. reaction rims are composed of quartz (Qtz), sillimanite (Sil), biotite (Bio), rimming garnet (Gar) cores. Reaction rims are 2-4 cm wide with 3 mm- 20 mm wide garnet cores. (B) Higher magnification photomicrograph of garnet from figure 2-3b (ppl), of pelitic schist with Reaction rim cored by garnet.

## **Ultramafic Rocks**

### **Macroscopic Description and Field Relations**

Ultramafic rocks in the southern Peacock Mountains are dark green to black, coarse grained, and locally contain a weak foliation. The ultramafic rocks are associated with mafic gneiss and metasedimentary rocks and occur as lenses between 3 m to 5 m thick and 10 to 20 m long.

### **Petrology**

The ultramafic rocks are characterized by the mineral assemblage amphibole + olivine  $\pm$  orthopyroxene  $\pm$  clinopyroxene  $\pm$  biotite  $\pm$  chlorite  $\pm$  zircon (Fig. 2-5). Due to widespread retrogression of primary mafic phases to amphibole, it was not possible to assign specific rock names to the ultramafic rocks. Amphibole is porphyroblastic, euhedral, and randomly oriented or weakly oriented parallel to foliation. Amphibole is likely a retrograde phase replacing ortho- and clinopyroxene. Olivine is porphyroblastic, poikiloblastic, and highly fractured. Ortho- and clinopyroxene are typically fine grained. Chlorite is euhedral, randomly oriented, and is kinked and folded (Fig. 2-5). Uncommon biotite is fine to medium grained and euhedral.

### **Interpretation**

The origin of the ultramafic rocks in the Peacock Mountains remains unknown. Possible interpretations include: 1) cumulates of mafic magmas, or 2) xenolithic fragments of oceanic crust.

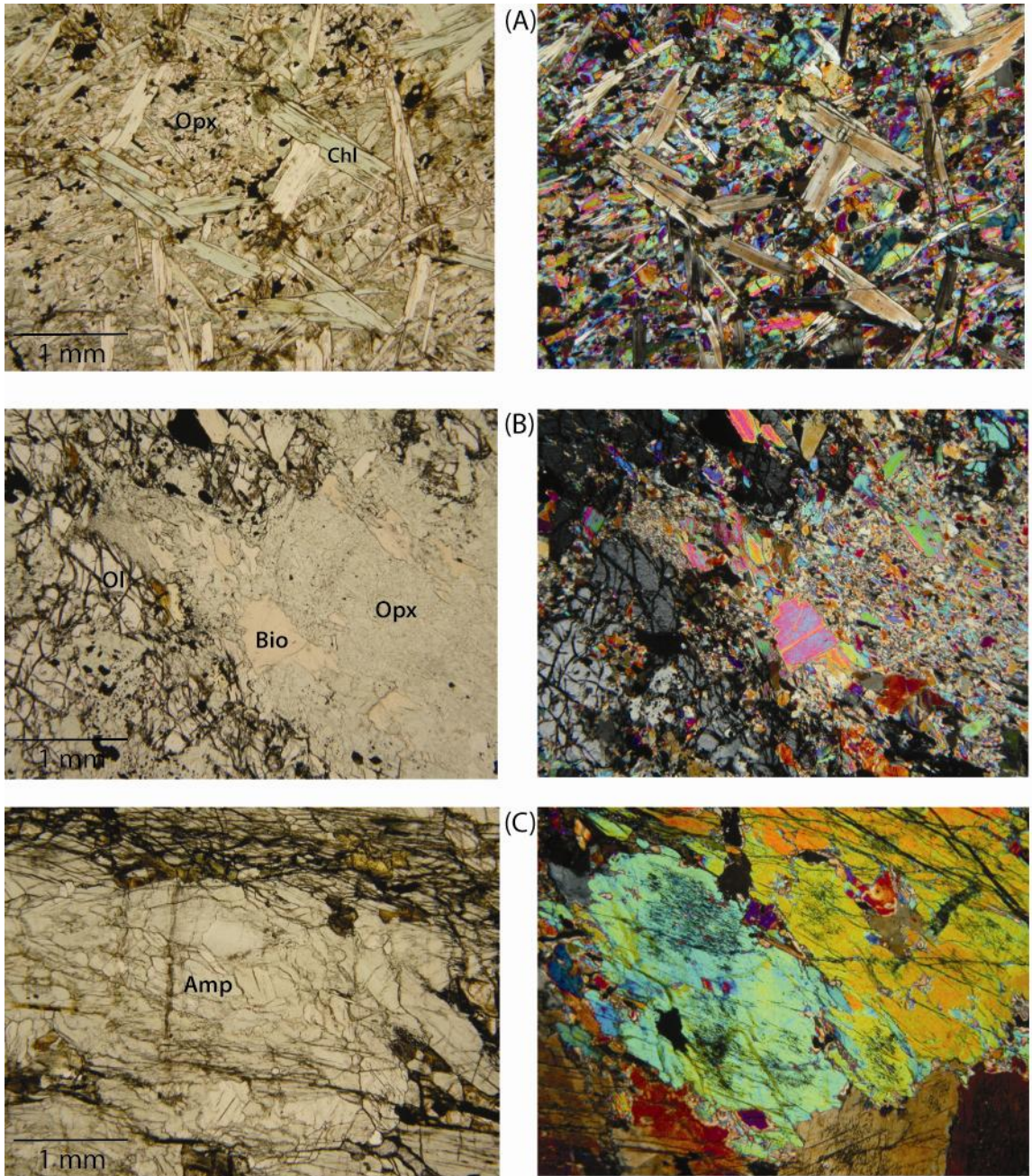


Figure 2-5: Photomicrographs of ultramafic rocks illustrating differences in mineralogy and texture (ppl left, xpl right). (A) sample MP 1/6/09-1, contains orthopyroxene (Opx), and chlorite (Chl), (B) and (C) sample MP 5/13/08-3, contains olivine (Ol), biotite (Bio), orthopyroxene (Opx), and amphibole (Amp).

## **Metamorphosed Plutonic and Volcanic Rocks**

### **Paleoproterozoic Mafic Gneiss (Xmg)**

#### **Macroscopic Description and Field Relation**

The mafic gneiss is mostly exposed in the northern and central sections of the map area (Plate 1). The mafic gneiss is dark gray to black, fine to coarse grained, strongly foliated and locally lineated. The mafic gneiss occurs as layers or lenses between 50 cm to 10 m thick. Some of the mafic gneiss contains 1-4 cm wide layers alternating from mafic rich to felsic rich (Fig. 2-6). However, not all outcrops contain the banding described above, and are instead homogeneous.

#### **Petrology**

The mafic gneiss is characterized by the mineral assemblage hornblende + plagioclase ± K-feldspar ± clinopyroxene ± quartz ± biotite ± olivine ± sphene ± apatite ± epidote ± calcite. Hornblende is medium to coarse grained, euhedral to subhedral, and porphyroblastic. Hornblende is commonly aligned parallel to the foliation and lineation (Fig. 2-7A). Plagioclase is medium grained, subhedral to anhedral, and locally has undulose extinction. In some samples plagioclase contains significant sericite alteration (Fig. 2-7B). Clinopyroxene is fine to medium grained and subhedral to anhedral. Quartz is fine grained, has undulose extinction, and tri-partate intersections at approximately 120° (Fig. 2-7B).

#### **Interpretation**

The mafic gneiss is interpreted to represent both mafic intrusions or flows and volcanogenic sediments. This interpretation is based on the absence of layering in some

of the mafic gneiss and the presence of compositional layering in other exposures (Figs. 2-7B, C). The protolith of the more heterogeneous outcrops is interpreted to be a volcanogenic sedimentary rock. This interpretation is based on the on the abundance of quartz in some samples, compositional layering, the interlayering of psammitic and pelitic schist (Figs. 2-1, 2-7B, C), and the presence of calcite. The texturally homogeneous mafic gneiss is interpreted to represent mafic intrusions or flows (Fig. 2-7A). This interpretation is based on mineralogy and the lack of compositional layering. It was not possible to distinguish between intrusions or flows during the course of this study, as no definitive features were found to differentiate between the two.



Figure 2-6: (A) Field photograph of mafic gneiss, facing west, looking at a vertical face. 1-4 cm wide alternating mafic rich and felsic rich layers have been interpreted to represent highly transposed primary compositional bedding. This leads to the interpretation that portions of the mafic gneiss may represent compositionally immature sediments.

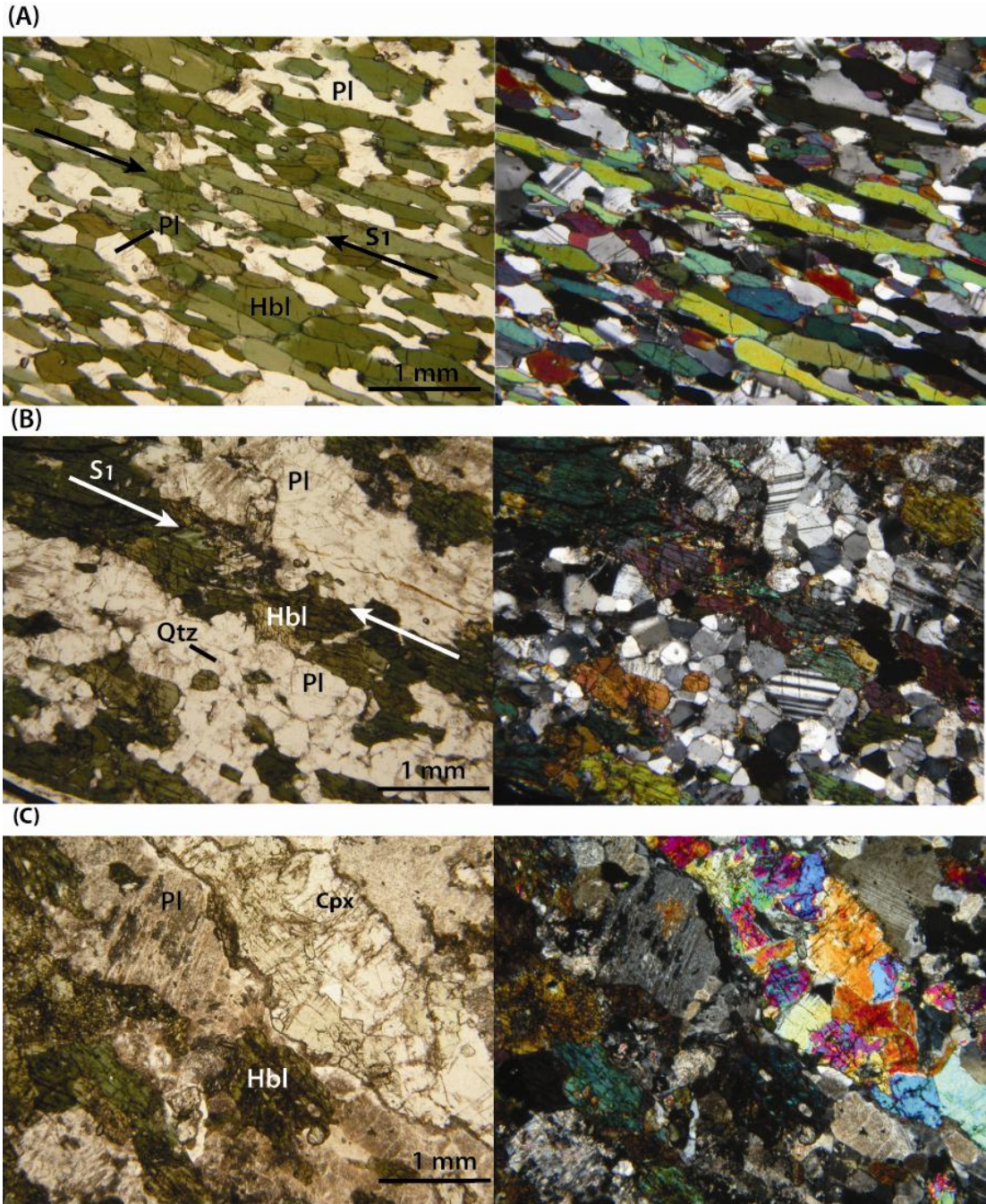


Figure 2-7: Photomicrographs of mafic gneiss (ppl left, xpl right). (A) MP 5/26/08-6, homogeneous mafic gneiss with hornblende (Hbl) and plagioclase (Pl) grains aligned parallel to S1. Sample does not contain compositional (gneissic) banding and the protolith interpreted to as a mafic volcanic rock. (B) and (C) MP 12/12/08-2, heterogeneous mafic gneiss with gneissic banding with felsic- and mafic-rich layers. Sample contains quartz (Qtz), plagioclase, hornblende, and clinopyroxene (Cpx). The presence of quartz and abundant plagioclase has been interpreted to represent possible volcanogenic sediment.

## **Paleoproterozoic Undifferentiated Granite (Xgr)**

### **Macroscopic Description and Field Relation**

The undifferentiated granite consists of several granitic rock types present in the map area. The majority of the undifferentiated granite is exposed in the northern and western parts of the map area (Plate 1). The undifferentiated granite is light pink and forms steep slopes and blocky outcrops. The unit is foliated, locally lineated, and medium to coarse grained. The undifferentiated granite appears to have intruded into the metasedimentary schist and mafic gneiss based on crosscutting relations. The undifferentiated granite contains quartz + plagioclase + K-feldspar ± biotite ± hornblende ± garnet. Plagioclase is abundant and generally medium to coarse grained. K-feldspar is medium to coarse grained and is commonly present as phenocrysts that range from 3 mm to 4 mm in size. Quartz is generally less abundant than plagioclase and K-feldspar, is fine to medium grained, and commonly defines the foliation and lineation. Biotite varies in abundance throughout the unit from absent to abundant. Biotite is fine grained and commonly defines the foliation and lineation. Hornblende is medium grained and typically defines the foliation and lineation. Garnet is uncommon and fine to medium grained.

### **Interpretation**

Based on crosscutting relationships the Paleoproterozoic undifferentiated granite is interpreted to be younger than the metasedimentary schist and mafic gneiss units. Additionally, the observation that the Paleoproterozoic undifferentiated granite contains the foliation, folds, and lineation, leads to the interpretation that the unit is pre- to syntectonic with respect to the local deformation.

## **Paleoproterozoic Megacrystic Granite (Xgrm)**

### **Macroscopic Description and Field Relation**

The megacrystic granite is exposed in the northern section of the map area (Plate 1). The megacrystic granite is light pink to gray and forms steep slopes and blocky outcrops. The megacrystic granite is poorly foliated and medium to very coarse grained and porphyritic. This granite intruded into the metasedimentary schist and mafic gneiss based on crosscutting relations.

The megacrystic granite contains quartz + K-feldspar + biotite + plagioclase. K-feldspar crystals are randomly oriented, euhedral phenocrysts between 2 cm and 3 cm long (Fig. 2-8). Plagioclase is medium to coarse grained and subhedral. Quartz is less abundant than K-feldspar and plagioclase and is medium grained. Quartz grains are elongate and define the foliation. Biotite is fine to medium grained and defines the foliation.

### **Interpretation**

Based on crosscutting relations, the Paleoproterozoic megacrystic granite is interpreted to be younger than the metasedimentary schist and mafic gneiss units, and to be younger than or coeval with the Paleoproterozoic undifferentiated granite. Because the Paleoproterozoic megacrystic granite contains the same foliation and folds as the wall rock, the unit has been interpreted to be pre- to syntectonic with respect to local deformation.

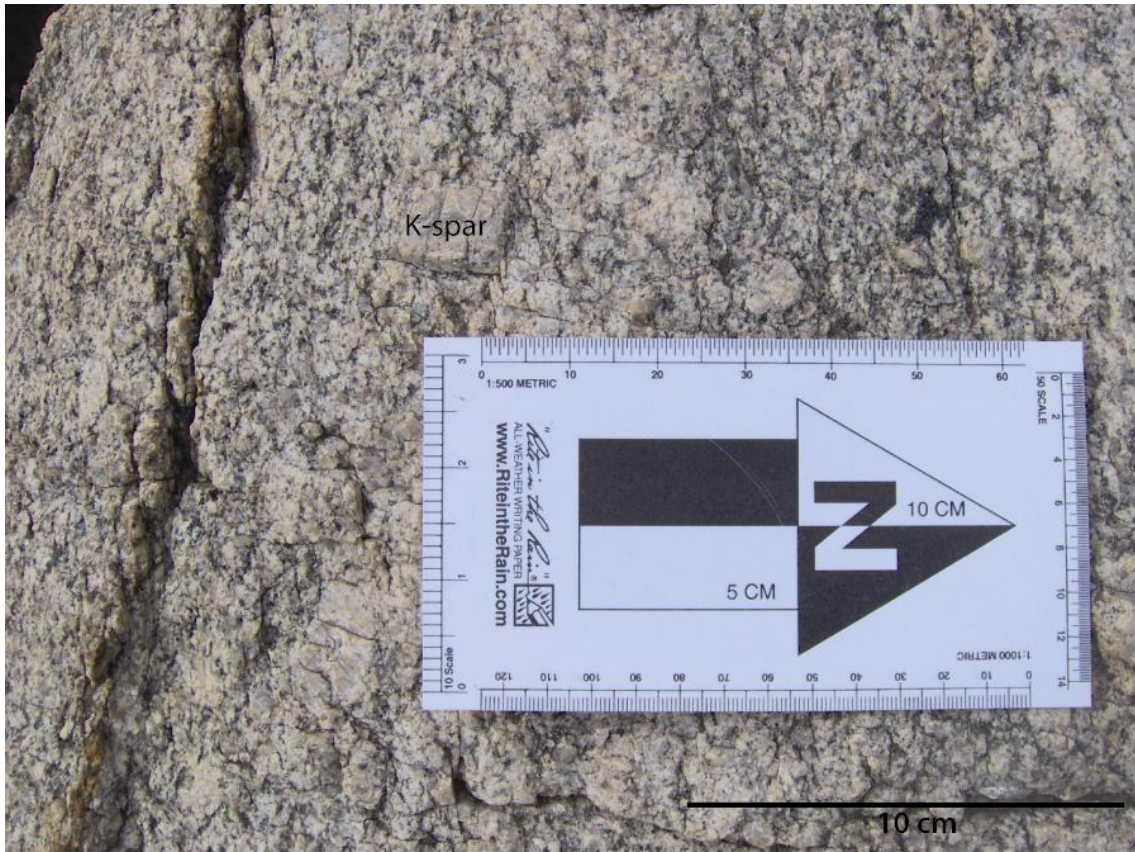


Figure 2-8: Field photograph of megacrystic granite, facing west, looking at face sloping to the east. Note 0.5-4 cm K-feldspar (K-spar) phenocrysts and foliation defined by biotite.

## **Unmetamorphosed Plutonic and Volcanic Rocks**

### **Paleo-Mesoproterozoic Undifferentiated Granite (XYgr)**

#### **Macroscopic Description and Field Relation**

The Paleo- Mesoproterozoic undifferentiated granite is exposed in the eastern section of the map area (Plate 1). The undifferentiated granite is pink to light pink and forms steep slopes and blocky outcrops. The unit is undeformed and medium to coarse grained. The undifferentiated granite intruded into the metasedimentary schist and mafic gneiss along a sharp contact and crosscuts the foliation in the older units (Fig. 2-9).

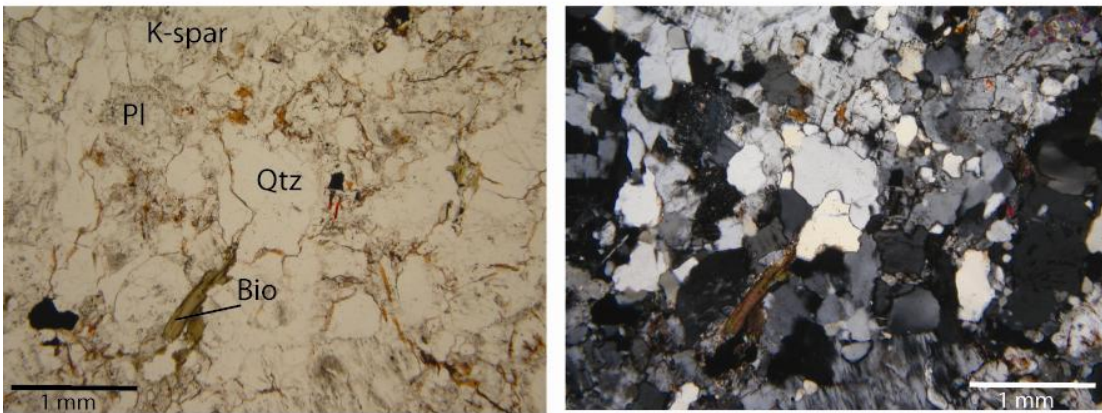
The undifferentiated granite contains K-feldspar + plagioclase + quartz + biotite + opaques + muscovite + garnet (Fig. 2-9). K-feldspar is coarse grained and anhedral. Plagioclase is medium to coarse grained and anhedral. Quartz is not as abundant as K-feldspar or plagioclase, has undulose extinction, is medium grained, and anhedral. Biotite is fine grained, anhedral, and randomly oriented. Garnet occurs as a trace mineral and is anhedral. Muscovite is fine grained and randomly oriented.

#### **Interpretation**

The Paleo-Mesoproterozoic undifferentiated granite has been interpreted to post-date both D<sub>1</sub> and D<sub>2</sub> deformations, based on the lack of any deformational fabric and the observed crosscutting of the foliation present in the metasedimentary schist (Fig. 2-9). The absolute age of the unit is unknown; however, voluminous anorogenic magmatism occurred in the southwestern United States at approximately 1.4 Ga (Van Schmus et al., 1996; Windley, 1993; Karlstrom and Humphreys, 1998). It is possible that the Paleo-

Mesoproterozoic undifferentiated granite is associated with this enigmatic magmatic event.

(A)



(B)

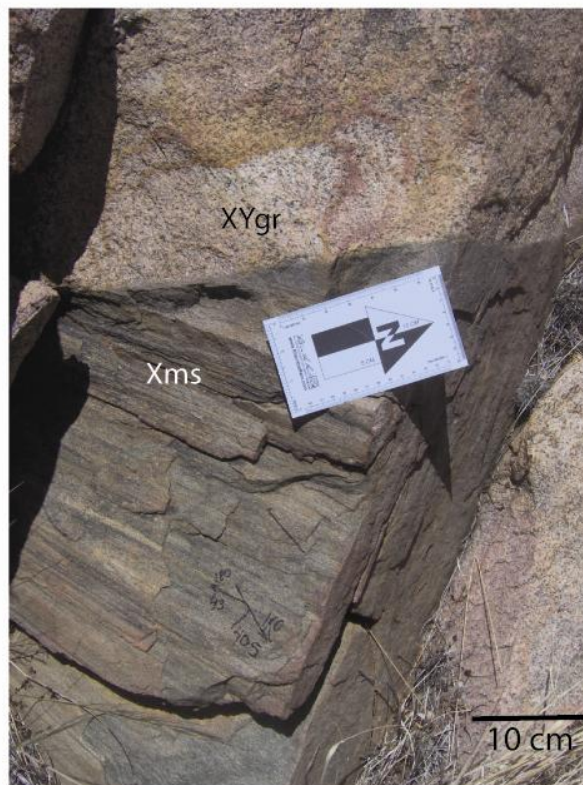


Figure 2-9: Photomicrographs of XYgr. (A) Photomicrograph of XYgr, ppl left, xpl right. (B) Field photograph of XYgr-Xms contact. Looking at face dipping to the south. Note truncation of foliation in schist by the granite.

## **Diabase Dikes (green stipple)**

### **Macroscopic Description and Field Relation**

Diabase dikes are exposed throughout the field area but they are volumetrically minor (Plate 1). These dikes are green to black, commonly form gentle slopes, crop out poorly, and are generally 3-10 m wide. The dikes intrude the metasedimentary schist, mafic gneiss, and undifferentiated granite. The orientation of the dikes is unknown due to poor exposure. Diabase dikes contain coarse-grained and randomly oriented, euhedral hornblende, clinopyroxene, plagioclase, and biotite (Fig. 2-10). Hornblende is porphyroblastic and approximately 2-10 mm long. Clinopyroxene is fine grained as present as cores in hornblende, suggesting the replacement of clinopyroxene by amphibole. Plagioclase is medium to coarse grained and commonly contains sericite alteration (Fig. 2-10). Biotite is fine to medium grained and randomly oriented.



Figure 2-10: Photomicrograph of diabase dike, ppl. MP 5/26/08-7 with hornblende (Hbl) phenocrysts and plagioclase (Pl).

## **Interpretation**

Based on similarities in mineralogy, texture, and outcrop pattern the diabase dikes are interpreted to be coeval with Mesoproterozoic diabase dikes and horizontal sheets in Arizona and California (Howard, 1991). Dikes and sheets have been dated at approximately 1100 Ma (Howard, 1999, and references therein). A diabase dike from the central Peacock Mountains yielded a U-Pb sphene date of approximately 1.08 Ga (Shastri et al., 1991). This date was interpreted as a crystallization age.

## **Tertiary and Quaternary rocks**

### **Tertiary Volcanic Rocks (Tv)**

#### **Macroscopic Description and Field Relation**

The Tertiary volcanic unit crops out in the southern and western margins of the map area (Plate 1). The Tertiary volcanic rocks are black to dark gray and form blocky, well exposed outcrops. The unit is composed of basalt and andesite that were not mapped separately during this study as they were not the focus of this work. No compelling evidence was found during the course of this study to suggest that the Tertiary volcanic unit is tilted more than 5-10°. This interpretation is based on the map pattern of the base of the unit.

## **Quaternary Alluvium (Qal)**

### **Macroscopic Description and Field Relation**

The Quaternary alluvium occurs throughout the field area in low lying areas and drainages. The Quaternary alluvium consists of poorly sorted, unconsolidated sediment with clasts that range in size from silt to boulder. Clasts are angular to subrounded and are mostly composed of the Paleoproterozoic rocks exposed in the field area.

## Chapter 3

### Structural Geology

#### Regional Deformation

Two Paleoproterozoic deformational events have been recognized in the southwest United States. These deformational events are designated as  $D_1$  and  $D_2$  in northwest Arizona. Similarly, two deformational events have been proposed in this study. However, the fabrics identified in this study differ in orientation from previously identified fabrics in northwest Arizona.

The earliest deformational event that has been identified throughout the southwestern United States ( $D_1$ ) is characterized by recumbent folds and a northwest-striking, gently northeast-dipping foliation.  $D_1$  has been dated at approximately 1740-1710 Ma in northwestern Arizona (Karlstrom and Bowring, 1988; Duebendorfer et al., 2001). The second deformational event that has been identified ( $D_2$ ) is characterized by a subvertical, northeast-striking foliation.  $D_2$  has been dated at approximately 1700-1685 Ma (Hawkins et al., 1996; Duebendorfer et al., 2001), and has been termed the Yavapai orogeny in Arizona and the Ivanpah orogeny in California.

#### Deformation in the Southern Peacock Mountains

##### Introduction

The Peacock Mountains contain evidence for two phases of deformation.  $D_1$  is characterized by a west- to northeast-striking, steeply-dipping foliation ( $S_1$ ), and steeply plunging isoclinal, intrafolial folds ( $F_1$ ) (Fig. 3-1).  $S_1$  foliation is axial planar to  $F_1$  folds that commonly fold late syn-tectonic quartz veins. The study area preserves evidence for

a second deformational event ( $D_2$ ) characterized by folds ( $F_2$ ) and a west- to northwest-trending lineation ( $L_2$ ) (Fig.3-1).  $F_2$  folds are open folds that plunge to the west-northwest. See Table 3 for the general characteristics of local and regional deformational events.

Deformation	Lineation	Foliation	Folds
$D_1$ Local	None	W to NE- striking, steeply dipping	Steeply-plunging isoclinal folds
$D_2$ Local	W-WNW-trending	none	W to NW-plunging open folds
$D_1$ Regional	Down dip	NW-striking, gently NE-dipping	Recumbent folds
$D_2$ Regional	Down dip	NE-striking, steeply dipping	Gently to moderately NE to SW-plunging tight to isoclinal upright folds

### Evidence for Polyphase Deformation

Considerable discussion has been focused on whether the two Paleoproterozoic fabrics in Arizona were produced by a single deformational episode (Karlstrom and Bowring, 1988; Bowring and Karlstrom, 1990; Albin and Karlstrom, 1991, Whitmeyer and Karlstrom, 2007) or separate orogenic events (Wooden and DeWitt, 1991; Duebendorfer et al., 2001; Duebendorfer et al., 2006). To determine if an area has undergone multiple phases of deformation it is necessary to identify different synkinematic mineral assemblages for each event and/or cross-cutting and overprinting relationships.

The Peacock Mountains contain two distinct generations of metamorphic fabrics, determined by overprinting relations. The map pattern of foliations suggests reorientation or overprinting of earlier foliation by later folding. Although there were no unequivocal

crosscutting relationships or re-folded folds observed in the field area, it is unlikely that the highly variable fabric orientations in the Peacock Mountains could have been produced by a single, protracted deformational event, as discussed below.

## **Paleoproterozoic Deformation**

### **S<sub>1</sub> Foliation**

The earliest fabric observed in the field area is designated as S<sub>1</sub>. The S<sub>1</sub> foliation is characterized by northeast to east-west strikes with moderate to steep, north, northwest, and southwest dips (Fig. 3-1, Fig. 3-2). The S<sub>1</sub> foliation is defined by an alignment of elongate quartz and platy biotite grains in the metasedimentary schist unit and by compositional banding of mafic and felsic minerals in the mafic gneiss. As stated in Chapter 2, the compositional banding is interpreted as highly transposed original bedding. The S<sub>1</sub> foliation is reoriented by F<sub>2</sub> folds about a steeply plunging, northwest-trending axis (Fig. 3-1) resulting in the variable strikes and dips. Because the S<sub>1</sub> foliation has been reoriented by later ductile deformation it is difficult to definitively determine the original orientation of the S<sub>1</sub> foliation. The S<sub>1</sub> foliation is axial planar to isoclinal, intrafolial, steeply plunging folds (F<sub>1</sub>) (Fig. 3-3).

Equal Area

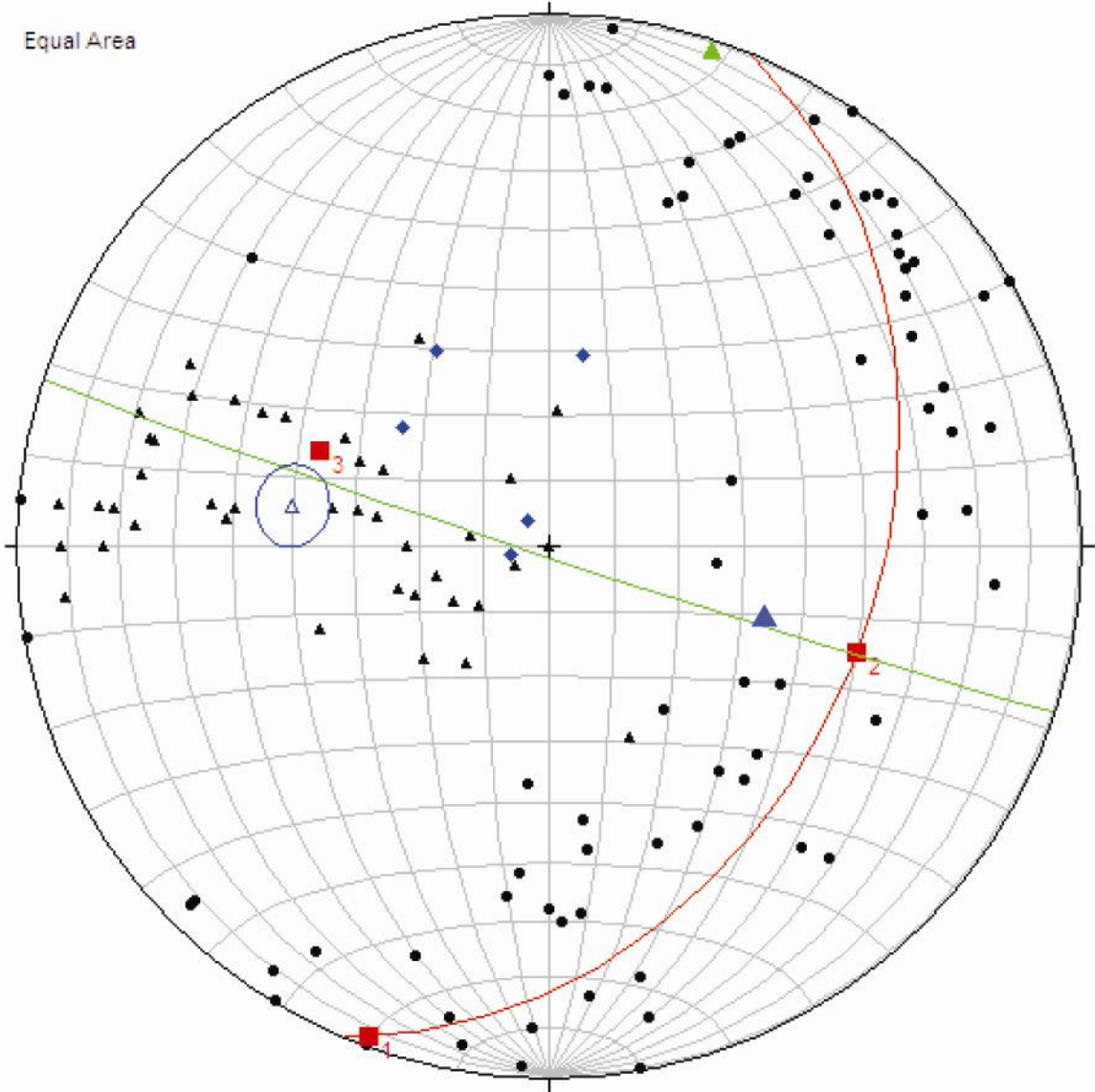


Figure 3-1: Equal area projection of poles to foliation (black dots), lineations (black triangles), mean lineation (blue triangle with blue circle),  $F_2$  fold axes (blue diamonds) and mean pole to foliation (blue triangle). Great circle best fit for the poles to  $S_1$  foliation (red) defines a  $\pi$  axis that plunges  $51^\circ$  to  $292^\circ$  and is interpreted to define the  $F_2$  fold axis.  $F_2$  axial surface (green) was chosen from the mean pole to foliation and axis of  $F_2$  folds (blue diamonds).

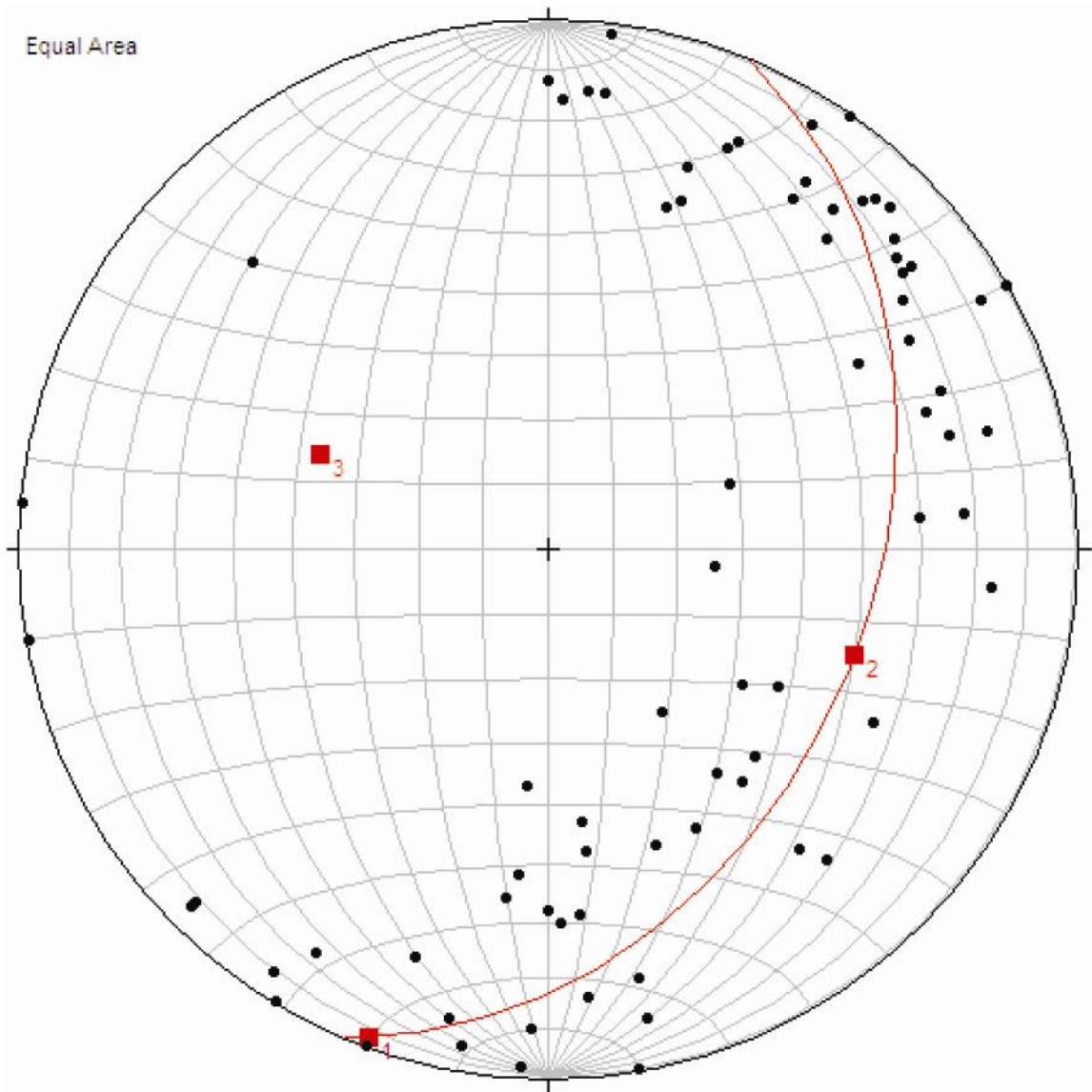


Figure 3-2: Equal area stereonet of poles to foliation ( $n= 168$ ), with best fit great circle (red). The pole to best fit great circle is interpreted to represent  $\Pi$  axis of  $F_2$  folds.

## **F<sub>1</sub> folds**

F<sub>1</sub> folds are present in the metasedimentary schist and mafic gneiss units where there are good markers such as layering and quartz veins to define folds. S<sub>1</sub> foliation is axial planar to F<sub>1</sub> folds. F<sub>1</sub> folds are isoclinal, intrafolial, steeply plunging, and fully transpose compositional layering interpreted as original bedding (S<sub>0</sub>) (Fig. 3-3). No systematic asymmetry was observed in F<sub>1</sub> folds.

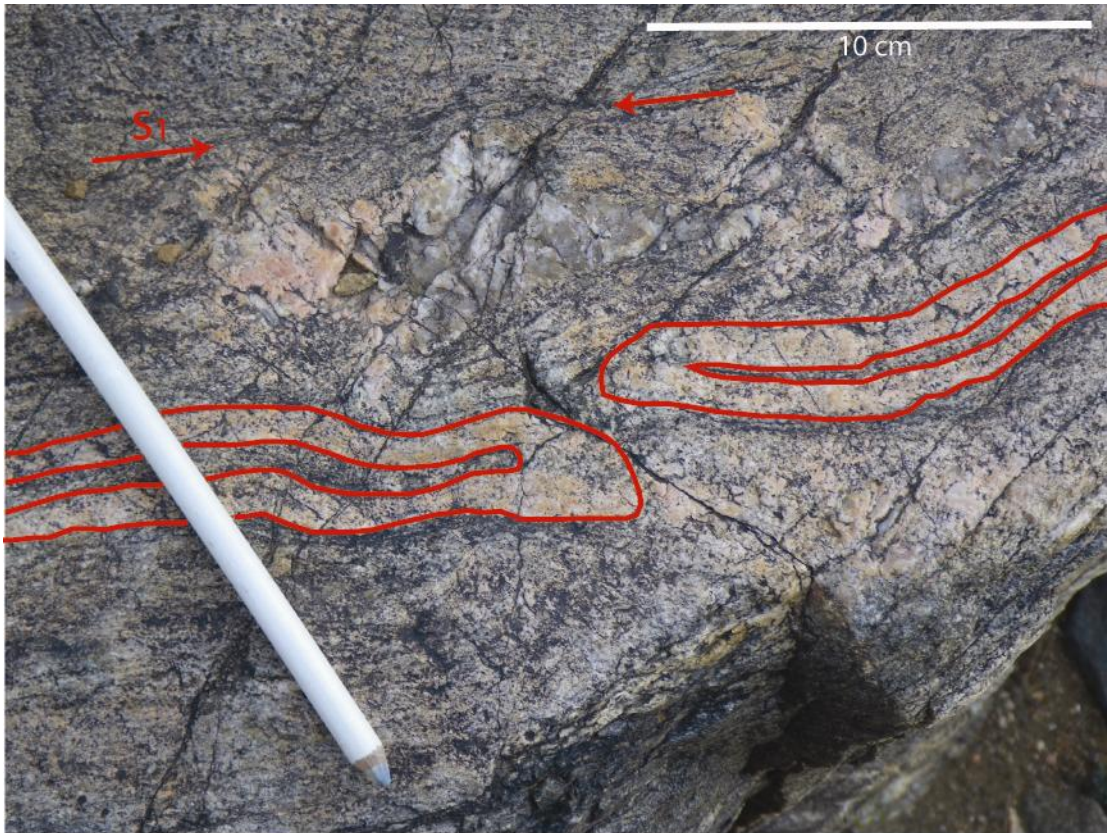


Figure 3-3: Annotated field photograph of isoclinal folds in psammitic schist. Pencil points north; downdip view of horizontal surface. Foliation is axial planar to folds. These have been interpreted to represent  $F_1$  folds and are fully transposed to the  $S_1$  foliation.

## **F<sub>2</sub> folds**

F<sub>2</sub> folds in the field area are west- to northwest-trending, steeply-plunging, tight to open folds (Fig. 3-4). F<sub>2</sub> folds fold the S<sub>1</sub> foliation (Fig. 3-4). F<sub>2</sub> folds are present as mesoscopic and macroscopic structures (Fig. 3-4, Plate 1). No evidence for an axial planar foliation or new mineral growth parallel to the axial surface of F<sub>2</sub> folds was observed. The orientation of F<sub>2</sub> folds is broadly consistent with north-south shortening.

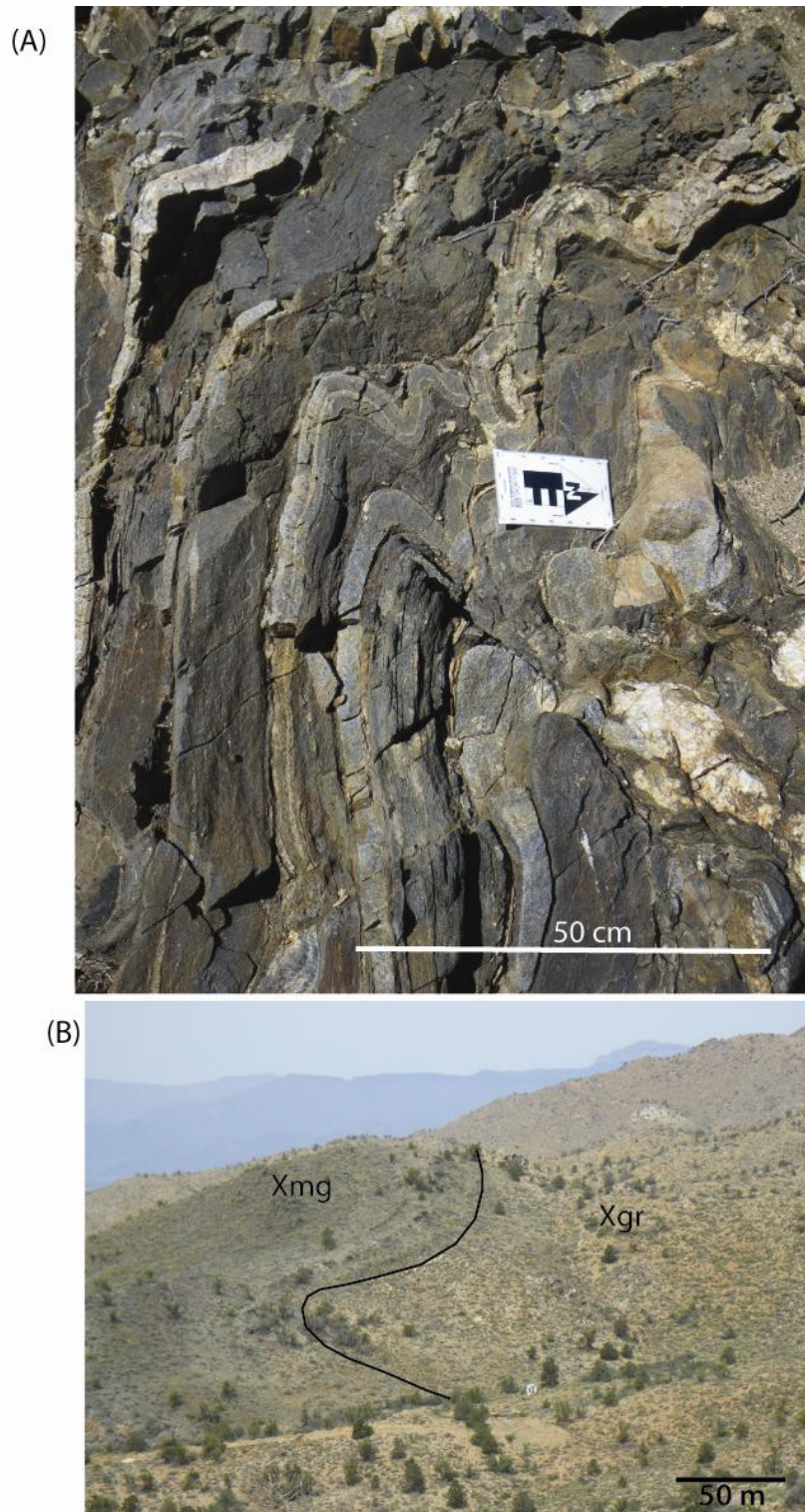


Figure 3-4: A) Field photograph of mesoscopic  $F_2$  folds in metasedimentary schist unit. Looking at a face sloping moderately to the southeast. Folded surface is  $S_1$  foliation. B) Field photograph of macroscopic  $F_2$  fold in undifferentiated granite (Xgr) - mafic gneiss (Xgm) contact. Photo looking north at face sloping to the south.

## **L<sub>2</sub> lineation**

Lineations in the field area are gently to steeply plunging and trend to the west and northwest (Fig. 3-5A, C). The lineation is defined by elongate aligned quartz, hornblende, and biotite grains and is subparallel to the axes of the F<sub>2</sub> folds (Fig. 3-1). Lineation trends are restricted to a relatively small range of strikes (Fig. 3-5B); however, the plunge ranges from subhorizontal to subvertical. It is not obvious from field observations alone whether these lineations are related to D<sub>1</sub> or D<sub>2</sub>. To determine whether the lineations are associated with D<sub>1</sub> or D<sub>2</sub>, and to resolve the issue of highly variable lineation plunges, a strike of foliation vs. rake of lineation plot was constructed (Fig. 3-6). The relatively small range in lineation trends is inconsistent with reorientation of a pre-existing lineation by a folding event. If a pre-existing lineation had been reoriented about the F<sub>2</sub> fold axis (51° toward 292°) one would expect a stereonet plot of lineation data to plot in one of three patterns based on the relative orientations of the original lineation with respect to the F<sub>2</sub> fold axis; these patterns are described below.

(1) If an original L<sub>1</sub> lineation was down dip and subparallel to the subsequent F<sub>2</sub> fold axis, then the lineation data would define a field with little scatter in trends and relatively uniform plunges. The lineation orientations would plot in a cluster subparallel to the F<sub>2</sub> fold axis. On a strike vs. rake plot, rakes would be lowest for strikes on the limbs of the fold, but would increase to 90° at the fold hinge, where strikes are perpendicular to the hinge. Because the F<sub>2</sub> fold hinge plunges toward 292°, strikes perpendicular to this orientation would be at 222° (or 020°). Figure 3-6 shows that, although four lineations with high rakes (60-80°) correspond with

this general strike direction, the overwhelming majority of steep rakes ( $>70^\circ$ ) correspond to strikes oriented between  $290^\circ$  and  $350^\circ$ ; i.e., at a high angle to  $222^\circ$ .

(2) If the original lineation was subparallel to the strike of  $S_1$  and orthogonal to the  $F_2$  fold axis, then the lineation data would define a great circle showing variable plunges, with the  $F_2$  fold axis defining the pole of the great circle. This is clearly not seen in the lineation orientation plot of Figure 3-5.

(3) If the original lineation was at an oblique angle to the fold axis, then the lineation data would define a small circle around the  $F_2$  fold axis with variable plunges. On a stereonet, strikes and plunges would show little scatter where the obliquity between the lineations and the fold axis is small (the limiting case being point 1 above). With increasing obliquity between the lineation and fold axis, the resulting small circle of lineations becomes larger with an increase in scatter between both the strikes of foliation and trends and plunges of lineation (the limiting case being point 2 above). On a strike vs. rake plot, there would be no systematic relation between strikes of foliation and trends of lineation.

Based on the stereonet plot in Figure 3-5 and the strike vs. rake plot in Figure 3-6 the lineation data are not consistent with any of the scenarios described above. The lineation data do not plot in a great or small circle distribution and have highly variable plunges, ruling out each of the above scenarios. It is noteworthy that, on the strike vs. rake plot (Fig. 3-6), rakes are generally low where strikes are  $260$ - $275^\circ$  but rakes increase where strikes become more northeasterly and northwesterly. This can be explained by lineation formation during or after  $F_2$  folding (Fig. 3-7). Low rakes (less than  $50^\circ$ ) corresponding to strikes between  $260$  and  $275^\circ$  (roughly east-west), and steep rakes

(greater than  $50^\circ$ ) corresponding to strikes between  $170-260^\circ$  and  $275-350^\circ$ , is consistent with formation of the lineation coeval with  $F_2$  folding. In addition, despite variable plunges, the lineation is subparallel to  $F_2$  fold axes and its trend is subparallel to the  $F_2$  axial surface (Fig. 3-1). For these reasons, I have interpreted the lineation in the Peacock Mountains to be associated with local  $D_2$  deformation, and therefore it is designated as  $L_2$ .

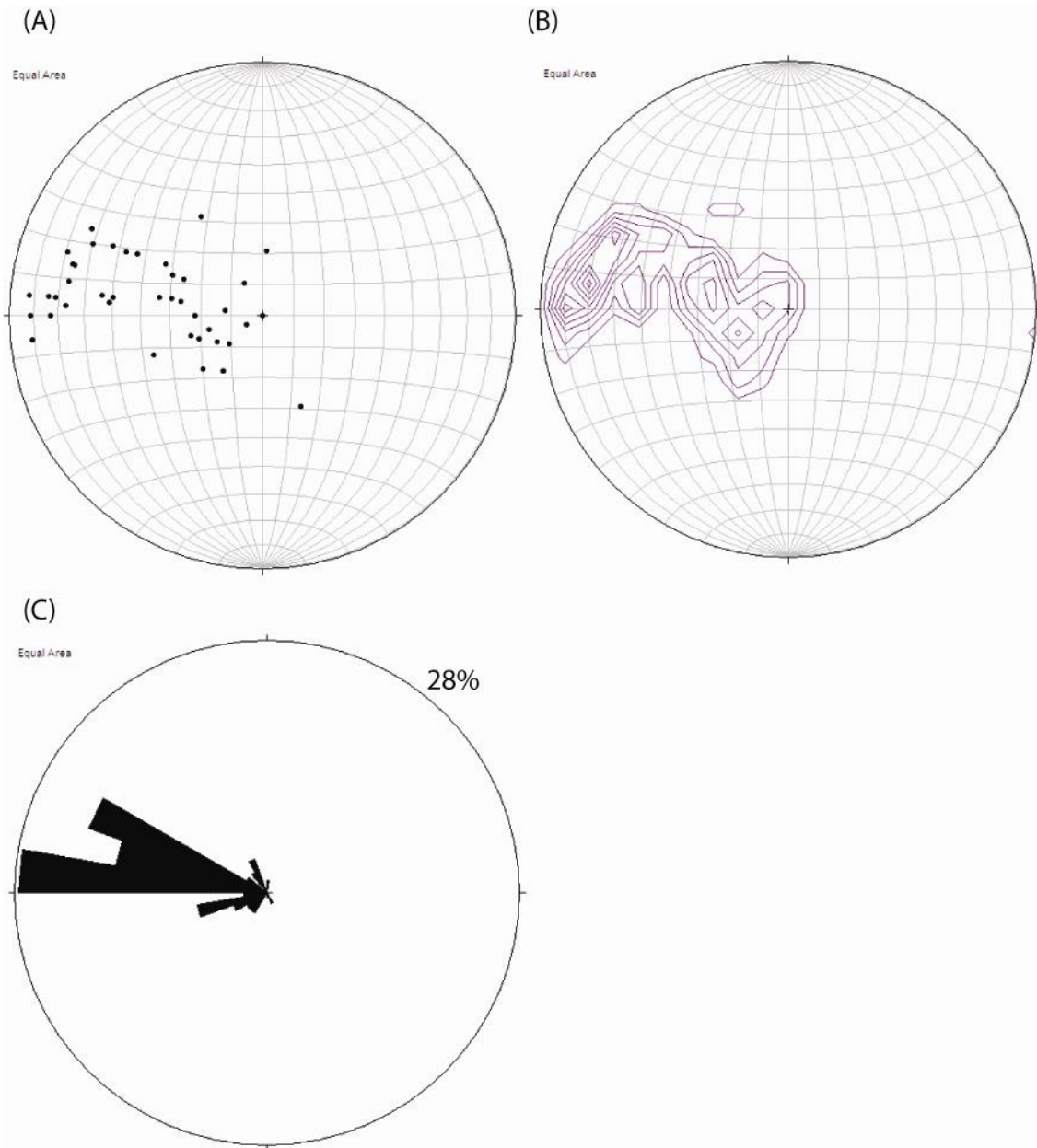


Figure 3-5: (A) Equal area stereonet plot of lineation (n= 76). (B) 1 % area contour of lineation data. (C) Rose diagram of lineation data (outer circle=28%).

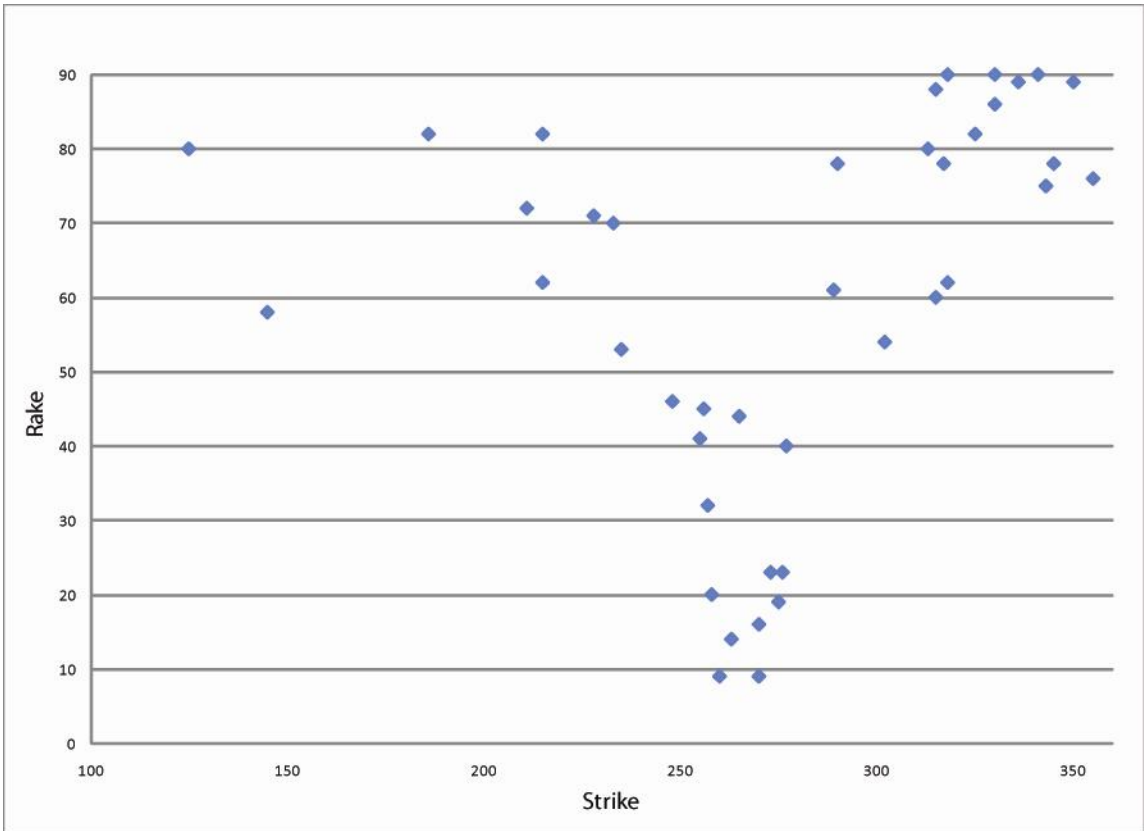


Figure 3-6: Strike vs. rake plot of lineation data from the Peacock Mountains (n=76). Note, variable rakes and Y shaped pattern with rakes less than 50° corresponding to approximately east-west (250-290°) strikes.

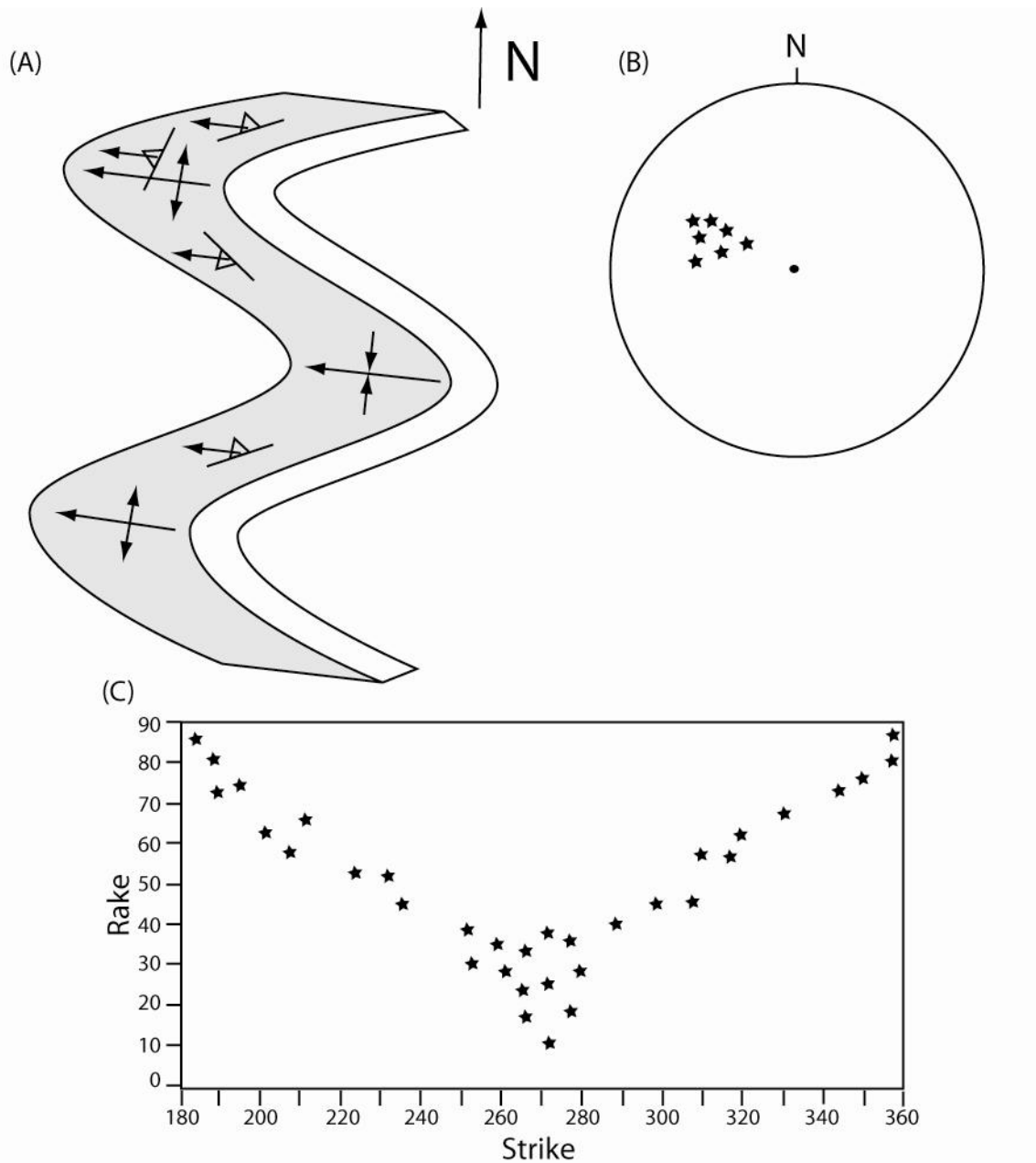


Figure 3-7: (A) Schematic line drawing of  $D_2$  folds with  $L_2$  lineation subparallel to fold axes. Note, consistent trend and plunge of lineations and variable rakes. (B) Schematic stereonet of lineation data predicted from A. (C) Schematic strike vs. rake plot predicted from A. Note, Y shape due to overprinting of lineation onto foliation surface rather than reorientation of preexisting lineation.

## **Interpretation and Conclusions**

Paleoproterozoic deformational fabrics in the Peacock Mountains are interpreted to not have been significantly reoriented by Tertiary extension. This is based on the lack of evidence for tilt in Tertiary volcanic rocks in the southern Peacock Mountains (Chapter 2, Plate 1). This interpretation is also supported by observations of limited tilt of Tertiary volcanic rocks on the eastern flank of the Cerbat Mountains (Orr, 1997). Additionally, this is supported by evidence presented by Faulds et al. (1997), where a deep (>2.5 km) extensional basin was documented in the Hualapai basin. However, this basin does not extend as far south as the Peacock Mountains and Cottonwood Cliffs, therefore extension and related tilt is likely to be relatively minor between the Peacock Mountains and Cottonwood Cliffs (Faulds et al., 1997).

Paleoproterozoic deformational fabrics in the central Peacock Mountains are similar to fabrics identified in the northern Hualapai Mountains (Siwec, 2003). In the northern Hualapai Mountains the  $S_1$  foliation (northwest-striking) has been attributed to regional  $D_1$  deformation (Siwec, 2003). In the Peacock Mountains this  $D_1$  foliation is attributed to regional  $D_1$  deformation. This is largely based on outcrop-scale similarities in structural style. Regional  $D_1$  deformation is characterized by a foliation and isoclinal, intrafolial folds, similar to  $D_1$  deformation in the Peacock Mountains (Karlstrom and Bowring, 1988; Orr, 1997; Duebendorfer et al., 2001).  $F_2$  folds and  $L_2$  lineations in the northern Hualapai Mountains have been attributed to a deformational event that occurred between the  $D_1$  and  $D_2$  regional deformational events (Siwec, 2003). The Peacock Mountains, however, do not contain fabrics that are consistent with regional  $D_2$  deformation (northeast-striking, steeply dipping foliation). However, Albin et al. (1991)

dated metamorphic zircon and sphene from amphibolite from the northern Peacock Mountains that were deformed by both local deformational events which yielded dates of 1.68 Ga. If the latest deformational event accompanied metamorphism, the data reported by Albin et al. (1991) are consistent with regional D<sub>2</sub> deformation (1700-1685 Ma) (Hawkins et al., 1996; Duebendorfer et al., 2001). The link between the reported date (1.68 Ga) and regional D<sub>2</sub> deformation is uncertain and therefore used with caution.

Based on the dates reported by Albin et al. (1991), similarities in principal shortening direction (approximately NW-SE), and similarities in structural style to deformation in the Cerat Mountains (moderately to steeply plunging folds and subparallel lineation)(Duebendorfer et al., 2001) I have attributed the local D<sub>2</sub> deformation to regional D<sub>2</sub> deformation. The differences in orientation of D<sub>2</sub> foliations and folds in the Peacock Mountains may be due to regional heterogeneities in principal stress directions during D<sub>2</sub> deformation or local variation adjacent to the large pluton in the northern section of the map area (Plate 1). Variations in the expression of regional D<sub>2</sub> deformation have also been documented in the southern Hualapai Mountains (Bonamici, 2007; Portis, 2009). Bonamici (2007) and Portis (2009) argue that the regional D<sub>2</sub> event is not well expressed in the southern Hualapai Mountains. In the Cerbat Mountains, Upper Granite Gorge of the Grand Canyon, and central Hualapai Mountains, D<sub>2</sub> fabrics are characterized by uniformly northeast-striking, steeply dipping foliation and intrafolial, upright folds (Ilg et al., 1996; Duebendorfer et al., 2001; Ferguson, 2002). In the areas listed above, D<sub>2</sub> deformation is well developed and pervasive, generally completely overprinting D<sub>1</sub> fabrics. However, in the Peacock Mountains and northern Hualapai Mountains D<sub>2</sub> deformation appears to be considerably less well developed because no

pervasive foliation formation accompanied  $F_2$  folding. Additionally the presence of map scale open folds similar to folds present in the Peacock Mountains suggests that the expression of  $D_2$  deformation may not be as consistent as previously documented (Fig. 3.8). The weak development of  $D_2$  fabrics may be due to the proximity of high-strength pre- to syn- $D_1$  plutons (Plate 1) and subsequent changes in the local stress field, or heterogeneities in the regional principal stress directions.

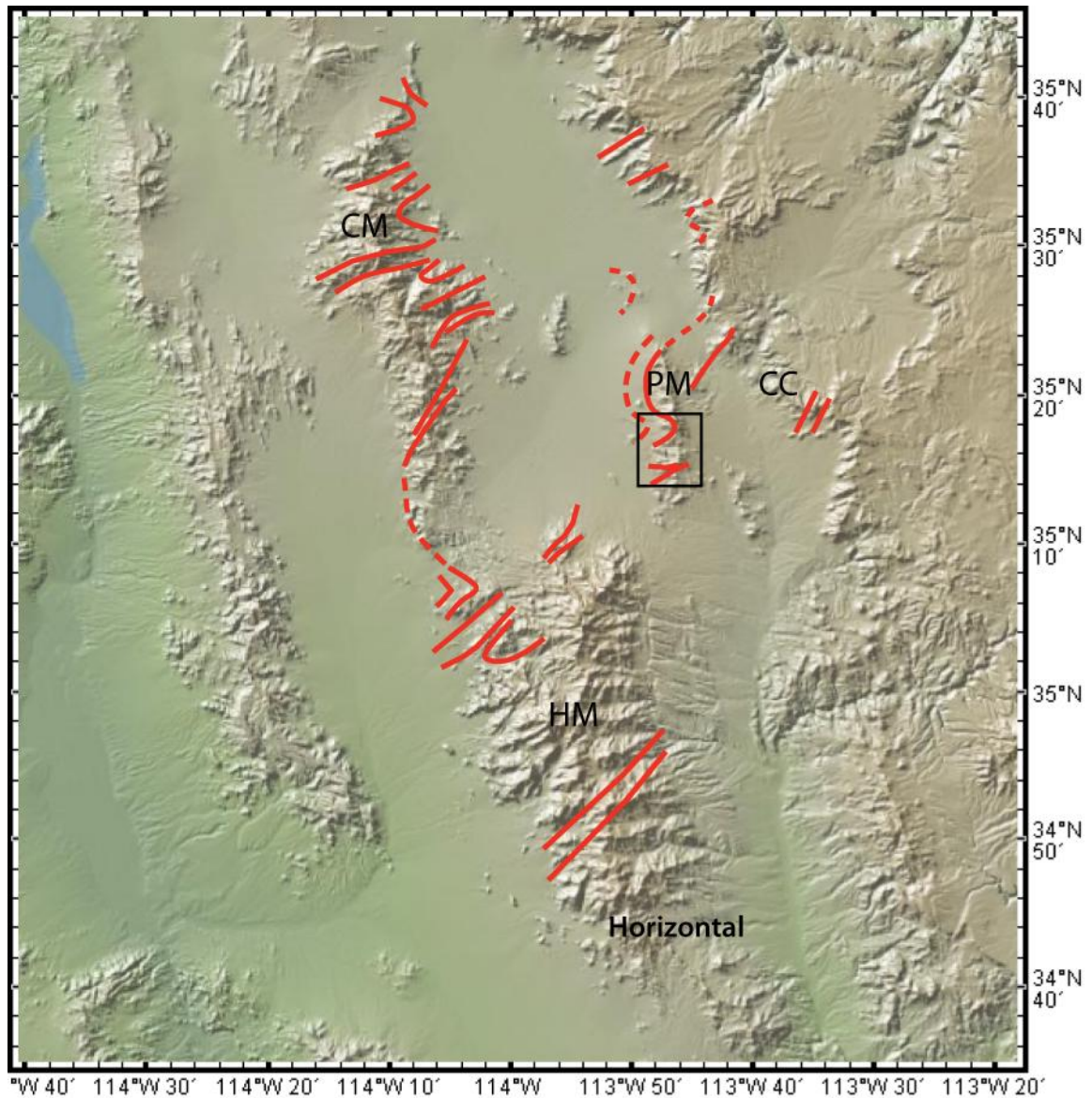


Figure 3-8: General foliation trajectory map of Paleoproterozoic foliation measurements from Northwest Arizona. Note large open folds in the northern Hualapai Mountains, Cerbat Mountains, Peacock Mountains, and Cottonwood Cliffs. In this study these folds have been attributed to regional  $D_2$  deformation (Albin, 1991; Evans, 1999; Duebendorfer et al., 2001; Siwiec, 2003; and Bonamici, 2007). Foliation measurements in the southern Hualapai Mountains are approximately horizontal (Bonamici, 2007; Portis, 2009). Field area located in black box. Cottonwood Cliffs (CC), Hualapai Mountains (HM), Cerbat Mountains (CM), and Peacock Mountains (PM).

## Chapter 4

### Conditions of Metamorphism

#### Introduction

The most abundant rock types in the field area include psammitic schist and granitic rocks, which do not contain appropriate mineral assemblages for the determination of pressure and temperature conditions of metamorphism. The pelitic schist contains mineral assemblages that broadly constrain pressure and temperature conditions of metamorphism. Mineral assemblages of pelitic rocks from the study area were plotted onto petrogenetic grids to semi-quantitatively determine metamorphic pressure and temperature.

#### Metasedimentary schist

Mineral assemblages of pelitic rocks from the field were used to qualitatively constrain the pressure and temperature conditions of metamorphism in the Peacock Mountains. Pelitic schist in the study area contains the assemblage garnet + sillimanite + K-feldspar + biotite + quartz  $\pm$  plagioclase + prograde and retrograde muscovite. Pelitic assemblages in the Peacock Mountains have been interpreted to record significantly lower pressure and temperature conditions than Paleoproterozoic rocks exposed in the Cerbat and Hualapai Mountains, but higher pressure and temperature conditions than the Cottonwood Cliffs directly to the east (Fig. 4-1) (Jones, et al., 1998; Evans, 1999; Duebendorfer et al, 2001; Siwec, 2003; Bonamici, 2007; Portis, 2009). The following sections describe the textures and inferred equilibrium conditions of relevant phases and interpretations of these features.

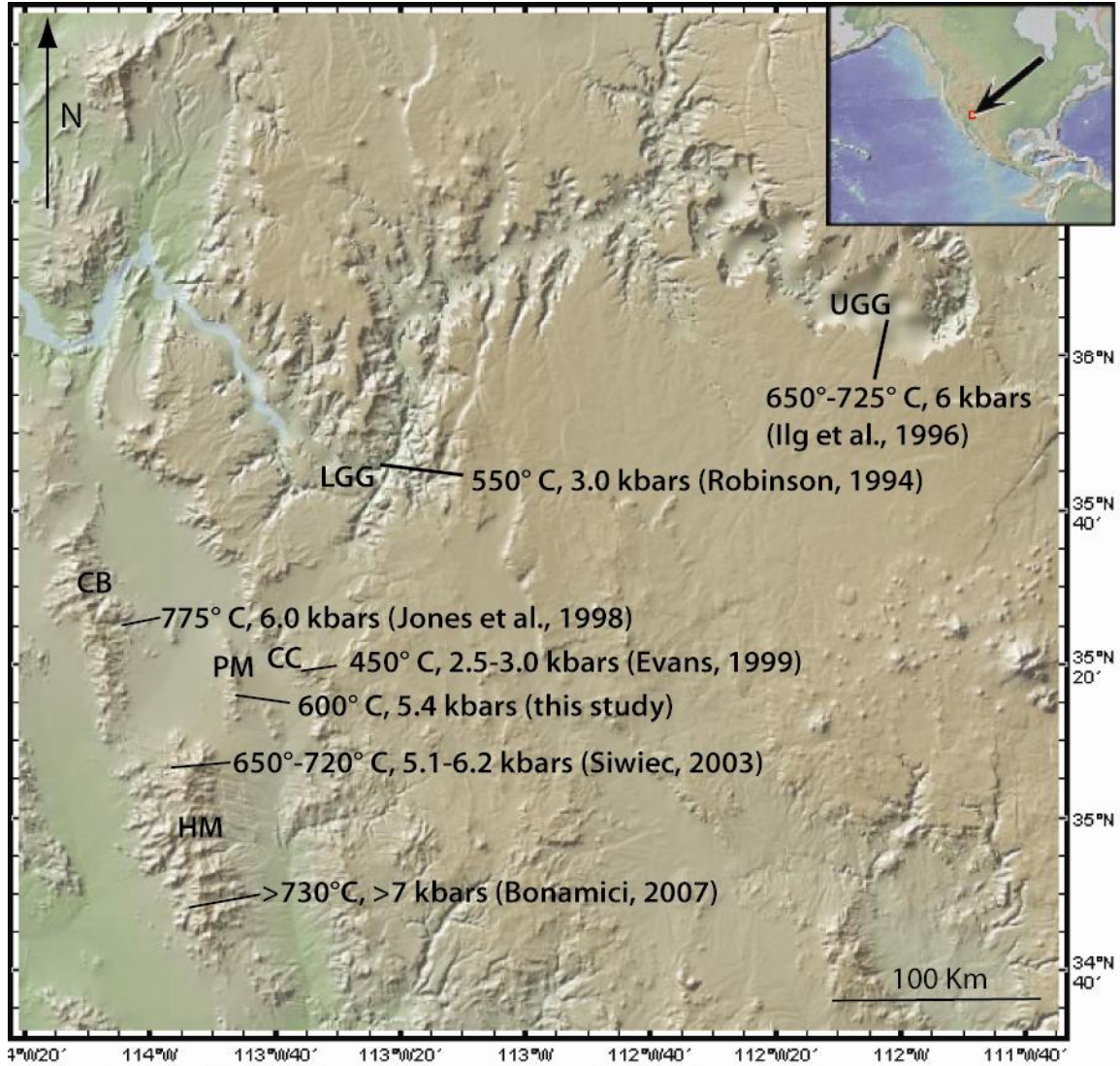


Figure 4-1: Shaded relief model image of northern Arizona with pressure and temperature conditions of metamorphism determined by garnet-biotite thermometry and GASP barometry. Note anomalously low pressure and temperature conditions in the southern Peacock Mountains (PM) and adjacent Cottonwood Cliffs (CC) compared to the Hualapai Mountains (HM), Cerbat Mountains (CM), Lower Granite Gorge (LGG), Upper Granite Gorge (UGG).

## **Garnet**

Garnet is porphyroblastic, commonly poikiloblastic, and subhedral to anhedral. Porphyroblasts range in size from 1 mm to 20 mm in diameter, with an average median size of approximately 3-4 mm in diameter (Chapter 2; Fig. 2-3). Porphyroblasts vary from poikiloblastic to inclusion free; quartz and biotite are the most common inclusions. Quartz inclusions are randomly oriented and commonly have an amoeboid shape; biotite inclusions are randomly oriented and euhedral (Chapter 2; Fig. 2-3). Porphyroblasts are randomly oriented and rimmed by quartz, sillimanite, and prograde and retrograde muscovite (Chapter 2; Fig. 2-3; Fig. 2-4).

## **Sillimanite**

Sillimanite is fibrous, fine to medium grained, commonly rims garnet, and is typically present as very fine-grained inclusions in quartz. Masses of sillimanite are randomly oriented and commonly form swirled aggregates (Chapter 2; Fig. 2-3). Sillimanite regularly occurs in reaction rims surrounding garnet porphyroblasts; however, sillimanite is not present as inclusions in garnet porphyroblasts.

## **Muscovite**

Muscovite is present in two distinct morphologies. Much of the muscovite is fibrous and fine grained. Some of the muscovite grains are euhedral and porphyroblastic. Muscovite porphyroblasts range in size from 0.5 mm to 1.5 mm in length. Muscovite

porphyroblasts are commonly present in rims around garnet porphyroblasts (Chapter 2; Fig. 2-3).

The fine-grained fibrous muscovite has been interpreted to represent a pseudomorph of sillimanite and therefore is a retrograde phase; however, the euhedral and porphyroblastic muscovite has been interpreted to represent a prograde phase, as it is aligned parallel with the foliation.

### **Biotite**

Biotite grains are euhedral to subhedral, and fine to medium grained. Biotite commonly occurs as euhedral, tabular inclusions in garnet porphyroblasts (Chapter 2; Fig. 2-3). However, biotite is absent from rims surrounding garnet porphyroblasts. Biotite is also present outside of the rims in the groundmass of the samples.

### **Interpretation**

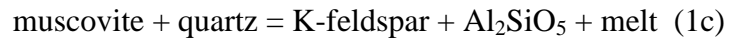
The presence of sillimanite, muscovite, and K-feldspar in equilibrium suggests that the reaction that produces K-feldspar and sillimanite has been crossed. This reaction creates a stability field between sillimanite, muscovite and K-feldspar (Fig. 4-2) (Thompson and Thompson, 1976; Spear et al., 1999).



The presence of muscovite and K-feldspar in equilibrium suggests that the muscovite breakdown reaction has not been crossed (Patiño-Douce and Johnston, 1991; Spear et al., 1999).



The lack of definitive evidence for partial melting places the assemblage on the low temperature side of the muscovite and quartz consuming and K-feldspar, sillimaite, and melt producing reaction (Spear et al., 1999).



Based on the interpretations of mineral assemblages listed above and inferred reactions the mineral assemblages observed are stable between temperature of 625° and 700° C and pressures of 3 kbars and 8 kbars (Fig. 4-2). These pressure and temperature conditions are consistent with upper most amphibolite facies conditions.

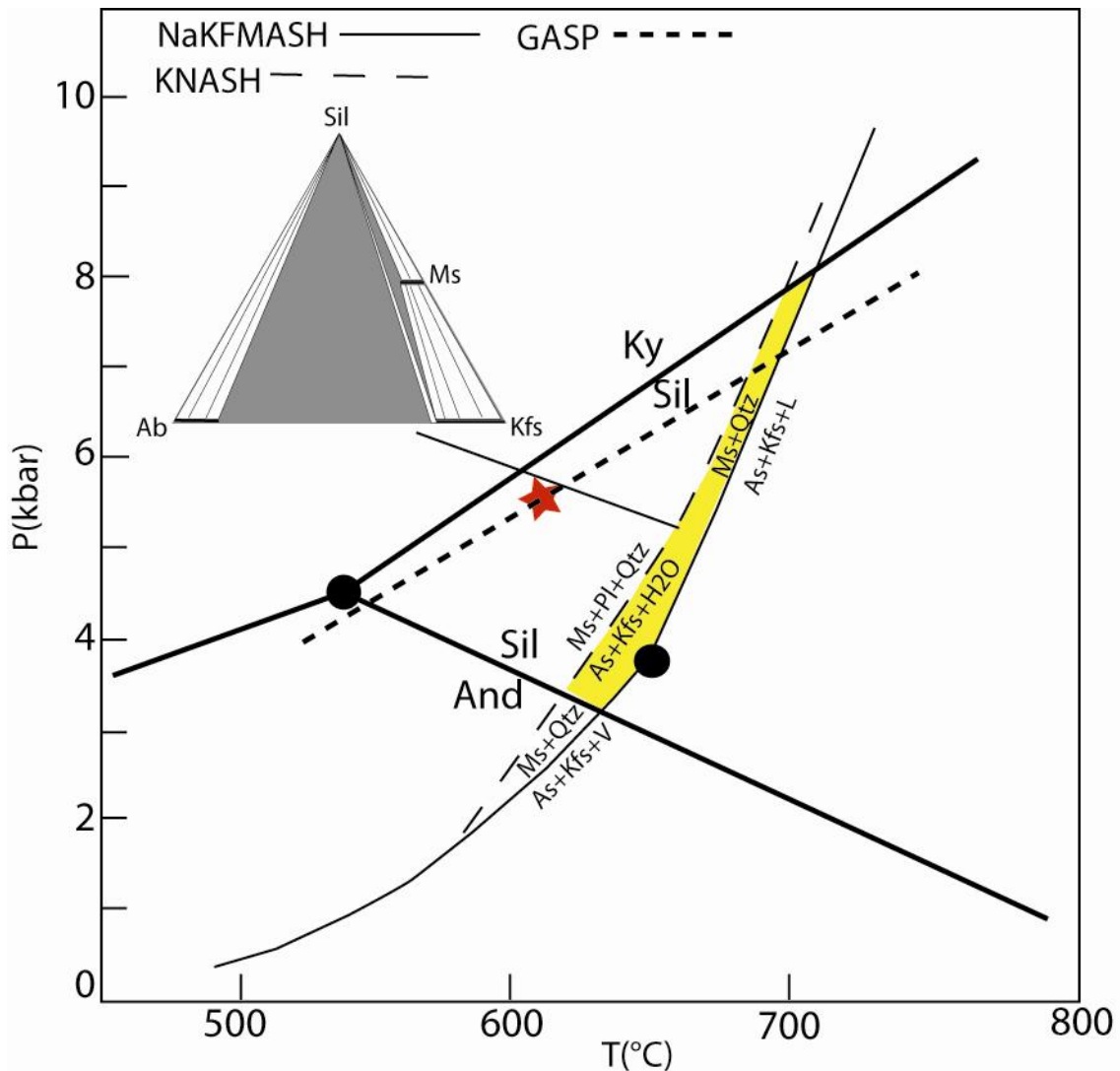


Figure 4-2: Petrogenetic grid with simplified NaKFMASH (solid lines), KNASH (long dash) systems (Spear et al. 1999; Thompson and Thompson, 1976). The red star represents approximate pressure and temperature conditions attained for sample MP 5/14/08-3 using the GASP barometer and garnet-biotite thermometer. Short dashed line represents projection of GASP barometer from sample MP 5/14/08-3. The mineralogy of samples; MP 5/14/08-1, MP 5/14/08-2, MP 5/14/08-3, MP 5/25/08-4, MP 5/26/08-2, MP 13/13/08-1B, MP 12/13/08-2 restricts them between the reactions muscovite + albite + quartz  $\rightarrow$  Kfs + As + H<sub>2</sub>O and muscovite + quartz  $\rightarrow$  Ksp + As + V. The lack of definitive evidence for partial melt textures limits the samples to the low temperature side of the Ms+Qtz  $\rightarrow$  As+Kfs+L reaction.

## **Thermobarometry**

### **Introduction**

The most abundant rock units in the field area are psammitic schist and plutonic rocks, neither of which contains the requisite mineral assemblages for quantitative thermobarometry techniques such as the GASP barometer and garnet-biotite thermometer. However, where pelitic schist with the requisite mineral assemblage (plag + qtz + bio + gar + sil) was present, samples were taken and thin sections were prepared. It is important to mention that the results presented here are preliminary and only represent one sample from the field area. Only one sample was analyzed due to mechanical problems related to the electron microprobe at Northern Arizona University.

### **Methods and Results**

The Cameca MBX electron microprobe at Northern Arizona University was used to determine mineral compositions in sample MP 5/14/08-3. The electron microprobe was operated with an accelerating voltage of 15 KeV, beam current of 10-25 nA, spot size of 1-15  $\mu\text{m}$ , and counting times between 30 and 33 seconds. The iron in biotite was assumed to be 15% ferric. A summary of the microprobe data collected in the course of this study are located in Appendix B. The garnet-biotite geothermometer of Holdaway (2000) and the garnet-aluminosilicate-plagioclase (GASP) geobarometer of Holdaway (2001) were used. Between 5 and 10 points were taken from individual garnet grains from sample MP 5/14/08-3. Points were taken from both garnet cores and rims. It was interpreted that no significant zoning exists in the composition of garnet grains based on

the uniformity of data obtained from cores vs. rims (Appendix B). The data from the points taken were averaged and pressure and temperature conditions were calculated.

A temperature of 600° and a pressure of 5.4 kbars were calculated for sample MP 5/14/08-3 (Fig. 4-3). These temperature conditions are low for the assemblages observed; therefore, these anomalous conditions have been interpreted to represent retrograde conditions, and are therefore considered to represent minimum pressure and temperature conditions (Fig. 4-2). However, due to low grossular and anorthite content in sample MP 5/14/08-3 the error associated with this result is in excess of  $\pm 4$  kbars, using the method described by Todd (1998) (Fig. 4-4). Because of the significant error associated this result is used with great caution.

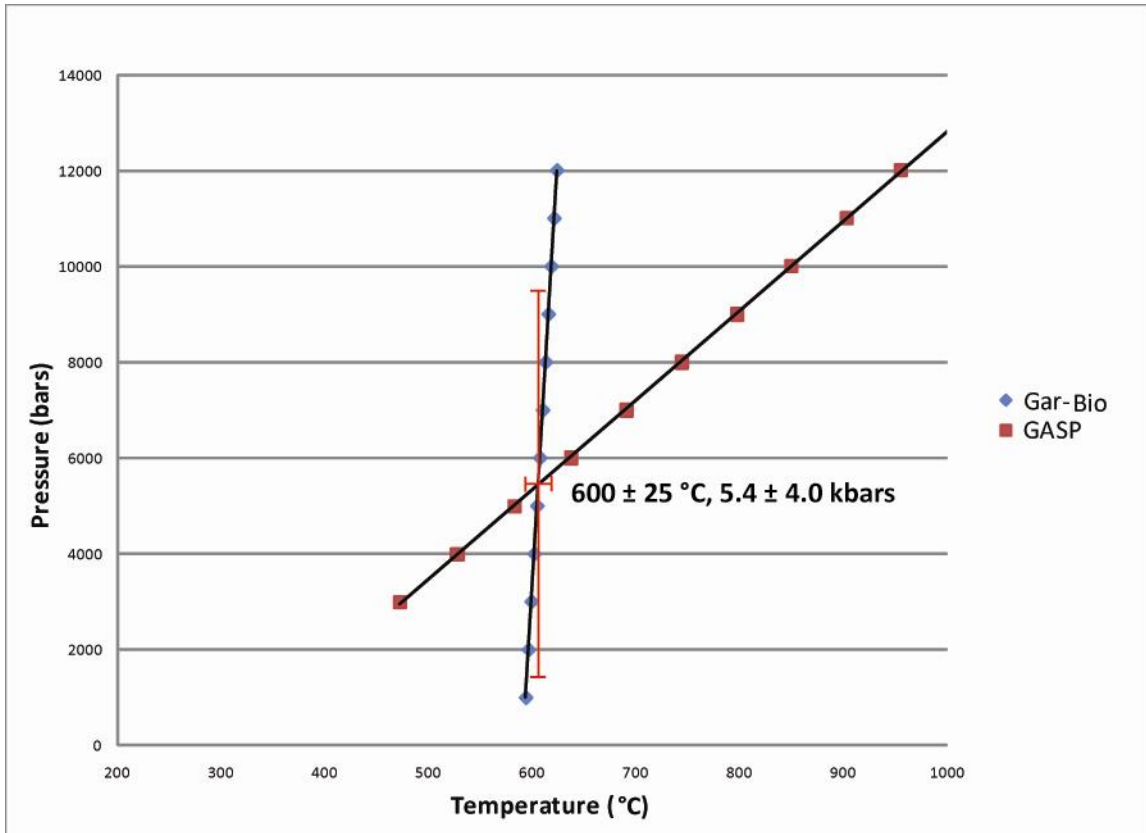


Figure 4-3: Garnet-biotite (gar-bio) geothermometry (Holdaway, 2000) and the garnet-aluminosilicate-plagioclase (GASP) geobarometry of (Holdaway, 2001), from sample MP 5/14/08-3 pelitic schist. GASP and gar-bio intersect at  $600 \pm 25^\circ\text{C}$  and  $5.4 \pm 4.0$  kbars.

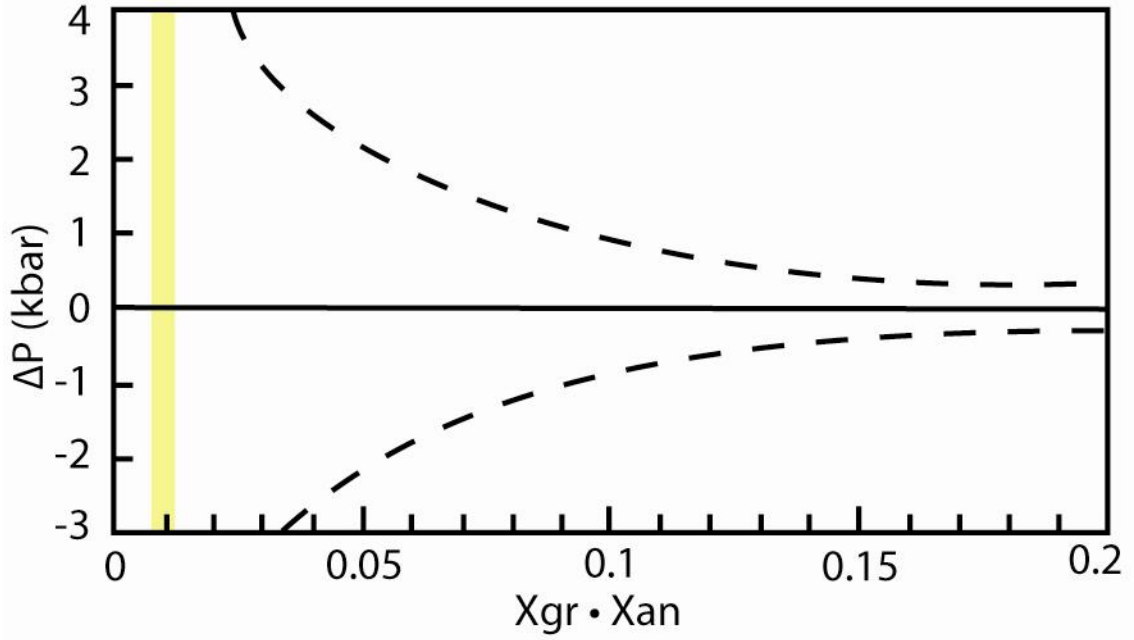


Figure 4-4: Error in GASP calculations resulting from low grossular and anorthite content. Yellow region represents approximate error in pressure determinations from sample MP 5/14/08-3. Error envelope developed by Todd (1998).

## **Conclusions and regional significance**

The pressure and temperature conditions of metamorphism in the Peacock Mountains (upper amphibolite facies) and Cottonwood Cliffs (upper green schist facies) are anomalously low when compared to surrounding ranges (Fig. 4-1). However, the minimum pressure and temperature conditions observed in this study are similar to conditions documented in the northern Hualapai Mountains (Siwec, 2003). The mineral assemblages observed do not aid in constructing a cohesive P-T path for the central Peacock Mountains. Additionally, due to the lack of geochronologic data on pre- or syn-deformational plutonic rocks in the field it is difficult to confidently associate metamorphism in the Peacock Mountains to regionally identified metamorphic events that were coeval with regional deformation (i.e. D<sub>1</sub>, vs. D<sub>2</sub>). Albin et al. (1991) reported U-Pb dates from metamorphic zircons and sphene of 1.68 Ga. If the date reported by Albin et al. (1991) is accurate, peak metamorphism in the Peacock Mountains is consistent in timing with D<sub>2</sub>-regional deformation (1700-1685 Ma) (Hawkins et al., 1996; Duebendorfer et al., 2001).

## Chapter 5

### Tectonic Implications

#### Introduction

The presence of two Paleoproterozoic deformational events has been well documented in northern Arizona (Albin and Karlstrom, 1991; Ilg et al., 1996; Duebendorfer et al., 2001; Dumond et al., 2007). The earliest deformational event ( $D_1$ ) is characterized by recumbent folds and a northwest-striking, gently northeast-dipping foliation.  $D_1$  has been dated at approximately 1740-1710 Ma in northwestern Arizona (Karlstrom and Bowring, 1988; Duebendorfer et al., 2001). The second deformational event ( $D_2$ ) is characterized by a subvertical, northeast-striking foliation.  $D_2$  has been dated at approximately 1700-1685 Ma (Hawkins et al., 1996; Duebendorfer et al., 2001), and has been termed the Yavapai orogeny in Arizona and the Ivanpah orogeny in California.

Two deformational events have been documented in the Peacock Mountains. However, these deformational events are not similar in fabric style or orientation to deformations identified elsewhere in northern Arizona. The pressure and temperature conditions of metamorphism appear to be anomalously low in the Peacock Mountains, and the abundance of metasedimentary rocks in the Peacock Mountains is anomalously high (Plate 1). The abundance of quartz-rich metasedimentary rocks suggests proximity to a continental source (Mojave province?); the presence of volcanogenic sedimentary rocks (mafic gneiss) is consistent with a back-arc setting for the Peacock Mountains (discussed further below). The following sections describe the general characteristics of Paleoproterozoic rock types and deformation in individual ranges in northwestern

Arizona. Figure 5-1 is a general geologic map of the study area and surrounding ranges.

A summary of the geochronologic data this is pertinent to this discussion is presented in table 4. I also propose a possible tectonic model for the formation of Paleoproterozoic crust in the region.

Date	Method	Location	Author's interpretation	Tectonic implication	Study
1730±9 Ma	Zircon, M	Cottonwood Cliffs	Granodiorite, pre- D <sub>1</sub> ?	Pre-D <sub>1</sub> arc plutonism	Chamberlain and Bowring (1990)
1735±7 Ma	Zircon, M	NW Hualapai Mts.	Metarhyolite pre- D <sub>1</sub> ?	Pre-D <sub>1</sub> volcanism	Chamberlain and Bowring (1990)
1723 Ma No error reported	Zircon, M	NW Hualapai Mts.	Amphibolite pre-D <sub>1</sub>	Pre-D <sub>1</sub> volcanism	Chamberlain and Bowring (1990)
1730 Ma No error reported	Zircon, M	Cottonwood Cliffs	Amphibolite pre- D <sub>1</sub> ?	Pre-D <sub>1</sub> volcanism	Chamberlain and Bowring (1990)
1727±9 Ma	Zircon, M	Cottonwood Cliffs	Dacite, pre-D <sub>1</sub> ?	Pre-D <sub>1</sub> volcanism	Chamberlain and Bowring (1990)
1720±6 Ma	Zircon, M	Poachie Range	Metarhyolite, pre-D <sub>1</sub>	Pre-D <sub>1</sub> volcanism	Bryant et al. (2001)
1768±5.5 Ma	Zircon, M	Cerbat Mts.	Water Tank granite, pre- or syn-D <sub>1</sub>	Pre-D <sub>1</sub> arc plutonism	Duebendorfer et al. (2001)
>1728.7	NA	Cottonwood Cliffs	Deposition of clastic section	Pre-syn-D <sub>1</sub> sedimentation	Evans, 1999
1717 Ma No error reported	Zircon, M	NW Hualapai Mts.	Orthogneiss, syn-D <sub>1</sub>	Syn-D <sub>1</sub> arc plutonism	Siwec (2003)
1735±4.3 Ma	Zircon, M	Cerbat Mts.	Big Wash granite, late-syn-D <sub>1</sub>	Late-syn-D <sub>1</sub> arc plutonism	Duebendorfer et al. (2001)
1728.7±1.8 Ma	Zircon, M	Cottonwood Cliffs	Valentine granite, late-syn-D <sub>1</sub> ?	Late-syn-D <sub>1</sub> arc plutonism	Chamberlain unpublished data
1710-1692 Ma No error reported	Zircon, M	NW Hualapai Mts.	biotite granite, syn-D <sub>1</sub> ?	Syn-D <sub>1</sub> Arc plutonism	Chamberlain and Bowring (1990)
1721±2.4 Ma	Zircon, M	Cerbat Mts.	Chloride granite, post-D <sub>1</sub> , pre-D <sub>2</sub>	Post-D <sub>1</sub> , pre-D <sub>2</sub> arc plutonism	Duebendorfer et al. (2001)
1735.5±6 Ma	Zircon, M	Cerbat Mts.	Dacite sill, pre-regional D <sub>2</sub>	Post-D <sub>1</sub> volcanism	Duebendorfer et al. (2001)
1719±1.2 Ma	Zircon, M	Cerbat Mts.	Diana granite, pre-D <sub>2</sub>	Post-D <sub>1</sub> , pre-D <sub>2</sub> arc plutonism	Duebendorfer et al. (2001)
1694±14 Ma	Zircon, M	NW Hualapai Mts.	Antler 2-mica granite, syn- D <sub>2</sub> ?	Syn-D <sub>2</sub> arc plutonism	Chamberlain and Bowring (1990)
1689±10 Ma	Zircon, M	Cerbat Mts.	Metamorphism metacarbonate, syn-D <sub>2</sub>	Syn-D <sub>2</sub> arc plutonism	Duebendorfer et al. (2001)
1682.5±2.3 Ma	Zircon, M	Cerbat Mts.	Granite dike, post-D <sub>2</sub>	End of local D <sub>2</sub>	Duebendorfer et al. (2001)
1660±5 Ma	Zircon, M	NW Hualapai Mts.	Cooling of metamorphism	End of local D <sub>2</sub>	Chamberlain and Bowring (1990)
1655±4.3 Ma	Zircon, M	Cerbat Mts.	Cooling or metamorphism	End of local D <sub>2</sub>	Duebendorfer et al. (2001)

All dates presented in this table were determined using U-Pb geochronology using multigrain (M) analyses.

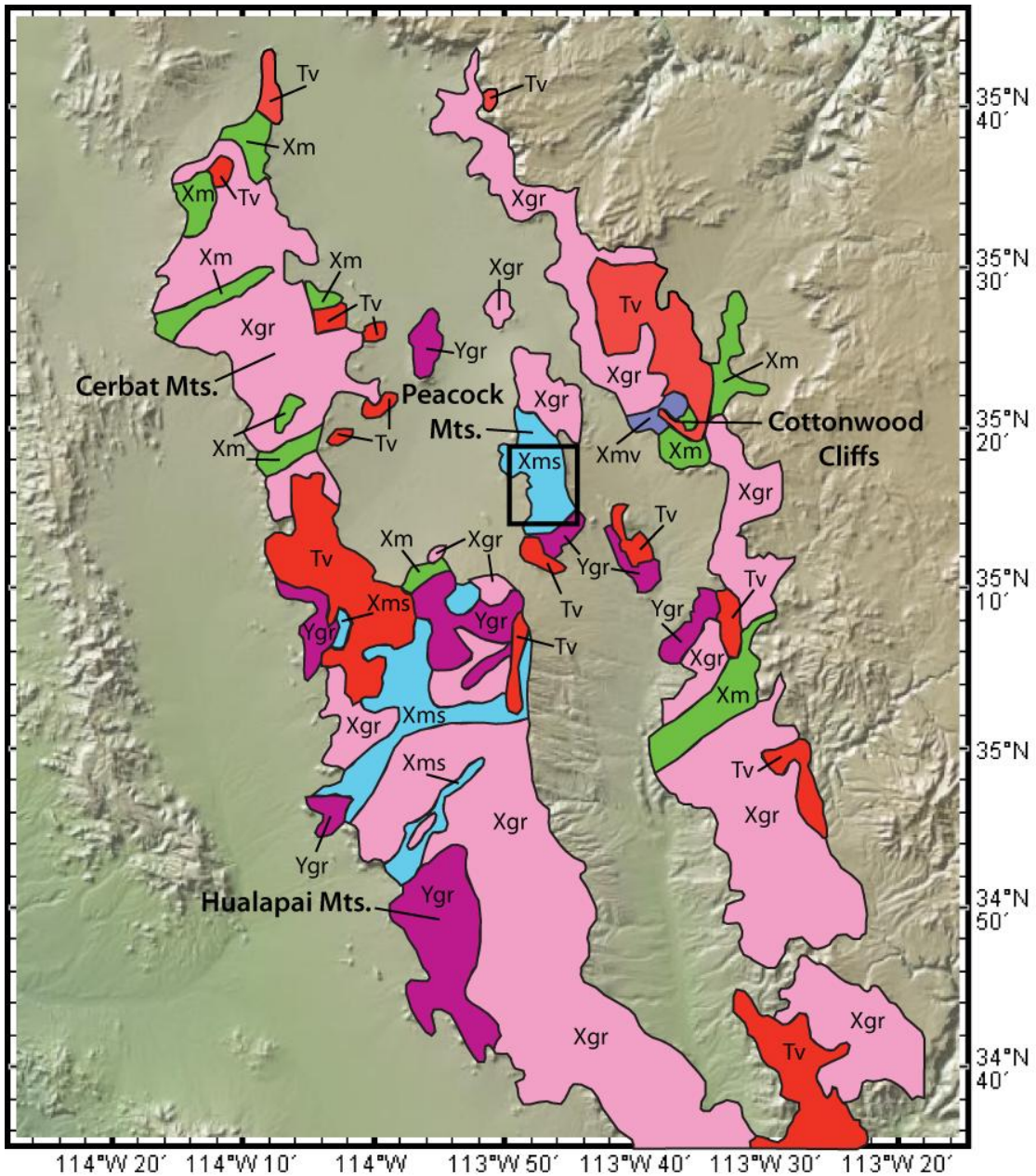
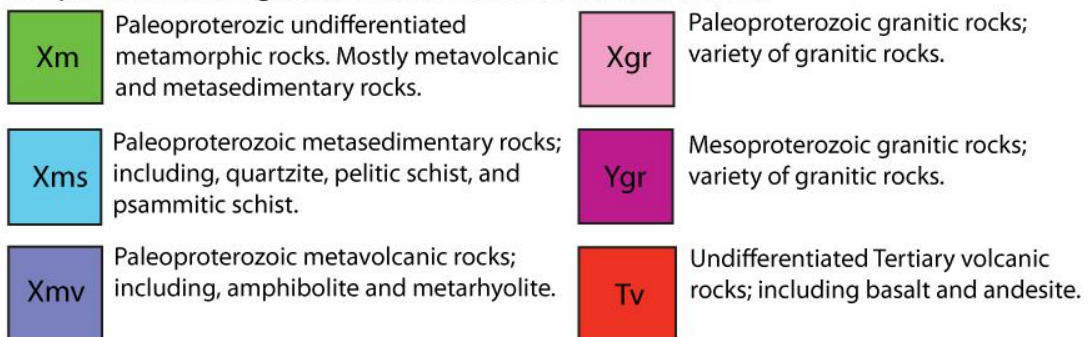


Figure 5-1: General bedrock geology map of the field area (box), and surrounding Paleoproterozoic ranges, modified from Richard et al. (2000).



## **Hualapai Mountains**

The northern Hualapai Mountains and Borianna Canyon area (central Hualapai Mountains) are dominated by plutonic and metavolcanic rocks with considerable amounts of metasedimentary rocks (Fig. 5-1) (Chamberlain and Bowring, 1990; Ferguson, 2002; Siwiec, 2003). The southern Hualapai Mountains are dominated by plutonic rocks that vary from felsic to mafic in composition and migmatitic gneiss, with minor amounts of amphibolite and metasedimentary rocks (Bonamici, 2007; Portis, 2009). The ages of Paleoproterozoic plutonic and metavolcanic rocks in the Hualapai Mountains range from  $1735 \pm 7$  Ma to  $1687 \pm 13$  Ma (Chamberlain and Bowring, 1990). Specifically, U-Pb zircon dates on metavolcanic rocks include a  $1735 \pm 7$  Ma on metarhyolite and 1723 Ma (no error reported) on amphibolite (Chamberlain and Bowring, 1990). The syn-D<sub>2</sub>, two-mica Antler granite yielded a U-Pb zircon age of  $1694 \pm 14$  Ma (Chamberlain and Bowring, 1990), which loosely constrains the age of D<sub>2</sub> deformation in the Hualapai Mountains.

The orientations of principal structural features of the northern and central Hualapai Mountains are broadly consistent with regional D<sub>2</sub> deformation. In the northern Hualapai Mountains D<sub>1</sub> fabrics are highly variable. This variability has been attributed to reorientation by D<sub>2</sub> deformation (Siwiec, 2003). The best fit pi axis for D<sub>2</sub> folding in the northern Hualapai Mountains plunges 64° towards 294°; this is similar to the best fit pi axis for D<sub>2</sub> folding in the Peacock Mountains (51°/292°). However, in the southern Hualapai Mountains a low-D<sub>2</sub>-strain window into regional D<sub>1</sub> and pre-D<sub>1</sub> deformation has been recognized, with sub-horizontal foliation (Bonamici, 2007; Portis, 2009).

Lead isotopic data from the Hualapai Mountains is consistent with evolved Mojave type (continental) crust (4.6-13.5  $\Delta J$ ), with isolated pockets of more juvenile (oceanic) components (2.4-3.8  $\Delta J$ ) (Wooden and Dewitt, 1991; Chamberlain, unpublished data).

### **Cerbat Mountains**

The Cerbat Mountains contain plutonic, metavolcanic, and metasedimentary rocks (Fig. 5-1) (Duebendorfer et al., 2001). Supracrustal rocks include amphibolite (metabasalt), garnet-biotite gneiss, quartzofeldspathic gneiss and very minor calc-silicate gneiss. These rocks have been intruded by a variety of plutonic rocks that range in composition from granite to granodiorite (Duebendorfer et al., 2001). The crystallization ages of plutonic and metavolcanic rocks in the Cerbat Mountains range from ca. 1765 Ma to  $1682.5 \pm 2.3$  Ma (Duebendorfer et al., 2001). The orientations of principal fabrics and macroscopic and mesoscopic structures are consistent with regional deformational fabrics (i.e.,  $D_1$  and  $D_2$ ) (Duebendorfer et al., 2001); with  $D_2$  structures dominating the southern and central Cerbat Mountains, and  $D_1$  fabrics, including west-vergent intrafolial recumbent folds, and north to northwest strikes and moderate dips (Duebendorfer et al., 2001).  $D_1$  fabrics in the Cerbat Mountains are highly variable; this variability has been attributed to incomplete transposition by  $D_2$  deformation (Duebendorfer et al., 2001).  $D_2$  fabrics in the Cerbat Mountains are characterized by a northeast-striking, subvertical foliation that is axial planar to upright folds. Folds plunge moderately to steeply northeast and are subparallel to a moderately to steeply plunging, east- to northeast-trending mineral elongation lineation (Duebendorfer et al., 2001).

In the Cerbat Mountains, the Water Tank Granite has been dated at 1765 Ma using U-Pb zircon geochronology (Duebendorfer et al., 2001). Duebendorfer et al. (2001) interpreted the Water Tank Granite to be pre- to syn-deformational with respect to D<sub>1</sub>. Additionally, the Big Wash Granite (pre- to early syn-D<sub>1</sub>) has been dated at 1737 ± 4.3 Ma (Duebendorfer et al., 2001). The widespread presence of metamorphosed pillow basalts (>1735 ± 6 Ma) in the Cerbat Mountains (Duebendorfer et al., 2001) is consistent with extension and limited marine incursion. Lead isotopic data from the Cerbat Mountains is consistent with evolved Mojave (continental) type crust, with Delta Jerome values ranging from 5.2 to 9.2 (Wooden and Dewitt, 1991; Chamberlain, unpublished data).

### **Cottonwood Cliffs**

The Cottonwood Cliffs are composed of plutonic, bimodal metavolcanic, and metasedimentary rocks (Fig. 5-1) (Albin and Karlstrom, 1991; Beard and Lucchitta, 1993; Evans, 1999). Plutonic rocks range in composition from granite to granodiorite (Beard and Lucchitta, 1993; Evans, 1999). A pre- to syn-D<sub>1</sub> granite/granodiorite pluton yielded a U-Pb zircon age of 1730 ± 9 Ma (Chamberlain and Bowring, 1990). This pluton intrudes a felsic metavolcanic unit (Evans, 1999). Additionally, dacite and amphibolite have been dated at ca. 1727 ± 8 Ma and 1730 Ma respectively, using U-Pb zircon geochronology (Chamberlain and Bowring, 1990). The amphibolite locally contains what have been interpreted to be deformed pillow basalts (Albin and Karlstrom, 1991; Beard and Lucchitta, 1993). The presence of deformed pillow basalts is consistent

with subaqueous volcanism in a marine setting. Additionally, the possible bimodal sequence described above is consistent with a rift-related volcanism.

The orientations of principal fabrics and structures are consistent with regional D<sub>2</sub> deformational features (Evans, 1999). D<sub>2</sub> deformation is more pervasive in the Cottonwood Cliffs than the aforementioned ranges; therefore, definitive evidence of fabrics related to an earlier event has not been documented in the Cottonwood Cliffs (Evans, 1999).

Lead isotopic data is consistent with juvenile to slightly evolved crust, with Delta Jerome values ranging from 0.5-3.8 (Wooden and Dewitt, 1991; Chamberlain, unpublished data).

### **Poachie Range**

The Poachie Range is dominated by plutonic and metavolcanic rocks with minor amounts of metasedimentary rocks (Bryant et al., 2001). Paleoproterozoic plutonic rocks range in composition from granite to gabbro (Bryant et al., 2001). The crystallization ages of metavolcanic rocks range from  $1730 \pm 12$  Ma to  $1718 \pm 6$  Ma (Bryant et al., 2001). Gabbroic and granodiorite plutons have been dated at approximately  $1711 \pm 22$ ,  $1721 \pm 6$ , and  $1680 \pm 10$  Ma using U-Pb zircon geochronology (Wooden and DeWitt, 1991; Bryant et al., 2001). Lead isotopic data from the Poachie Range and the area surrounding Bagdad, Arizona (Bagdad Block) are consistent with evolved to mixed type crust, with Delta Jerome values between 4.1 to 10.8 in the Poachie Range and 4.9 to 10.1 in the Bagdad Block (Wooden and Dewitt, 1991).

## **Central Arizona**

Plutonic rocks in and around Prescott, Arizona, have been dated between 1700 to 1750 Ma using U-Pb geochronology on zircons from pre- to syntectonic plutonic rocks (DeWitt, 1989). These plutonic rocks range in composition from tonalite to gabbro and intrude a sequence of metavolcanic and metasedimentary rocks that are presumed to range in age from 1720 to 1780 Ma (DeWitt, 1989). This metavolcanic-metasedimentary suite of rocks has been proposed to have been associated with island-arcs and associated marginal basins (C.A. Anderson and Silver, 1976; P. Anderson, 1978; 1986a, 1986b; P. Anderson, 1989; Karlstrom and Bowring, 1988). This interpretation is supported by lead isotopic data consistent with juvenile (oceanic) crust (-3.8 to 2.5  $\Delta J$ ). Based on major and minor trace element abundances and trends in relative abundances of incompatible minor elements from plutonic rocks, Dewitt (1989) suggested the presence of a northwest-dipping subduction zone between 1750 to 1700 Ma.

## **Tectonic Setting of the Peacock Mountains**

One of the goals of this study is to determine the original tectonic setting of the Peacock Mountains. Any proposed tectonic setting must account for depositional environments that explain: 1) the abundance of quartz-rich sandstones (psammitic schist), 2) less common shales and mudstones (pelitic schist), 3) volcanoclastic rocks (heterogeneous mafic gneiss), and 4) mafic or intermediate volcanism (homogeneous mafic gneiss).

An extensional back-arc setting is most compatible with the interpretations of metasedimentary and metavolcanic rocks in the field area. The expression of extensional back-arc basin sedimentation and volcanism is complex and diverse, and therefore

difficult to describe in a short discussion (Marsaglia, 1995). Extensional back-arc basin volcanism is characterized by lava flows, volcanic breccias, pyroclastic rocks, and reworked volcanoclastic material (Marsaglia, 1995). The presence of abundant basaltic sills and dikes in the Yamato Basin in the Japan Sea has been documented during the study of cores from ODP legs 127 and 128 (Thy, 1992). This basaltic material was intruded into sedimentary rocks that were sourced from both the volcanic arc and stable continent. These sedimentary rocks are dominated by several sedimentary facies as defined by Marsaglia et al. (1992). These facies are: 1) pelagic fallout, 2) air borne ash, and 3) submarine gravity flows, some of which may have initiated as pyroclastic flows that were reworked by aqueous processes. Extensional back-arc basins such as the Sea of Japan may receive sediment from both the frontal continental arc and the continental margin (Packer and Ingersoll, 1986; Marsaglia et al., 1992). The contribution of sediment from the continental margin results in increased quartz content in sedimentary rocks in the back-arc relative to the fore-arc and to an intra-oceanic volcanic arc (Packer and Ingersoll, 1986; Marsaglia et al., 1992).

The abundance of reworked volcanoclastic material, the presence of quartz-rich sediments, and the basaltic dikes, sills, and flows satisfy all of the requirements for an extensional back-arc depositional environment for the Peacock Mountains. Based on this interpretation, and similarities in sedimentation and volcanism, I have proposed an extensional back-arc basin as a probable tectonic setting for the Peacock Mountains and surrounding ranges (Fig. 5-2).

## **Tectonic Model**

In this section, I propose a tectonic model for the formation of the Mojave-Yavapai boundary zone, and the early deformational and magmatic history of the Paleoproterozoic orogen in northwestern Arizona. Tectonic models for crustal growth and assembly must address (1) the distribution of Pb isotope signatures, (2) tectonic settings that permit the early development of penetrative fabrics and burial to >18 km, (3) timing of deformational and magmatic events, and (4) the composition and distribution of major rock types.

Although no geochronology was conducted during the course of this study, some geochronologic data is available in the literature. See Table 4 for a summary of Paleoproterozoic plutonic rock ages from ranges surrounding the Peacock Mountains. Unfortunately, despite the relative high precision of U-Pb zircon dates, errors in the range of  $\pm 5$ -10 m.y. do not allow resolution or distinction of events that may be very closely spaced in time (e.g., tectonic switching from extension and crustal thinning to shortening and crustal thickening over time intervals < 10 m.y.; Collins, 2002).

The mechanism for tectonic switching that I propose for the back-arc extension in western Arizona during the Paleoproterozoic is similar to the mechanism proposed by Zorin et al. (2009), and Jones et al. (2009). In this model, back-arc extension is a result of slab roll-back or trench retreat (Zorin et al., 2009; Jones et al., 2009). In the tectonic model proposed here, the oldest granite and granodiorite plutons in the Cerbat Mountains and Cottonwood Cliffs represent the early continental-arc in Figure 5-2a. These oldest granitoids are approximately coeval with isotopically juvenile rocks in central Arizona (DeWitt, 1989). The evolved and mixed isotopic character of the Cerbat and Peacock

Mountains, respectively, suggests involvement of continental crust (Wooden and DeWitt, 1991). Additionally, the presence of detrital zircons in metasedimentary rocks and inherited zircons as old as 2.8 Ga in granitoids confirms the involvement of older crust (Wooden et al., 1994; Duebendorfer et al., 2001). Based on the coeval emplacement of plutonic rocks in the Cerbat Mountains, Cottonwood Cliffs, and central Arizona as well as the inferred northwest-dipping subduction zone (DeWitt, 1989), the geometry illustrated in Figure 5-2a has been proposed for the time period between 1750-1730 Ma.

In the tectonic model proposed here, the deformed pillow basalts (amphibolite) in the Cerbat Mountains and Cottonwood Cliffs (Duebendorfer et al. 2001; Albin and Karlstrom, 1991; Beard and Lucchitta, 1993) are interpreted to have been deposited in a back-arc basin that split the arc and may have formed due to slab roll-back. Additionally, the presence of bimodal metavolcanic sequences in the Cottonwood Cliffs and Hualapai Mountains, and to a lesser extent the Cerbat Mountains, is consistent with rift-related volcanism (Chamberlain and Bowring, 1990). These metavolcanic rocks have been dated at approximately >1735-1723 Ma using U-Pb geochronology on zircon (Chamberlain and Bowring, 1990; Duebendorfer et al., 2001). The presence of what have been interpreted to be back-arc basin metasedimentary rocks in the Peacock Mountains and northern Hualapai Mountains (Siwec, 2003) is also consistent with extension behind a continental-arc. In the tectonic model presented in this study, these metasedimentary and metavolcanic rocks are interpreted to have been deposited in a back-arc basin between 1735 and 1720 Ma (Fig. 5-2b).

In the final stages of the model presented in this study, plutonic rocks in the Poachie Range are interpreted to represent the second continental-arc after the closure of

the back-arc basin (Wooden and DeWitt, 1991; Bryant et al., 2001). The closure of the back-arc basin is thought to have been the result of increased coupling between the downgoing slab and the active arc, and the accretion of island arcs associated with the Yavapai province (Fig. 5-2c). This period of deformation would have produced the west-vergent recumbent folds in the Cerbat Mountains and the associated gently east-dipping D<sub>1</sub> foliation in both the Cerbat and southern Hualapai Mountains.

The closure of back-arc basins by the accretion of island arcs and subduction of oceanic plateaus has been documented in the Lachlan orogen of eastern Australia (Collins, 2002). The rapid and repeated alteration from extension (back-arc rifting) to contraction (accretion of terranes) is termed “tectonic switching” (Collins, 2002). This process is increasingly recognized as important in contractional orogenic belts (e.g., Lister and Forster, 2009; Zorin et al., 2009; Jones et al., 2009).

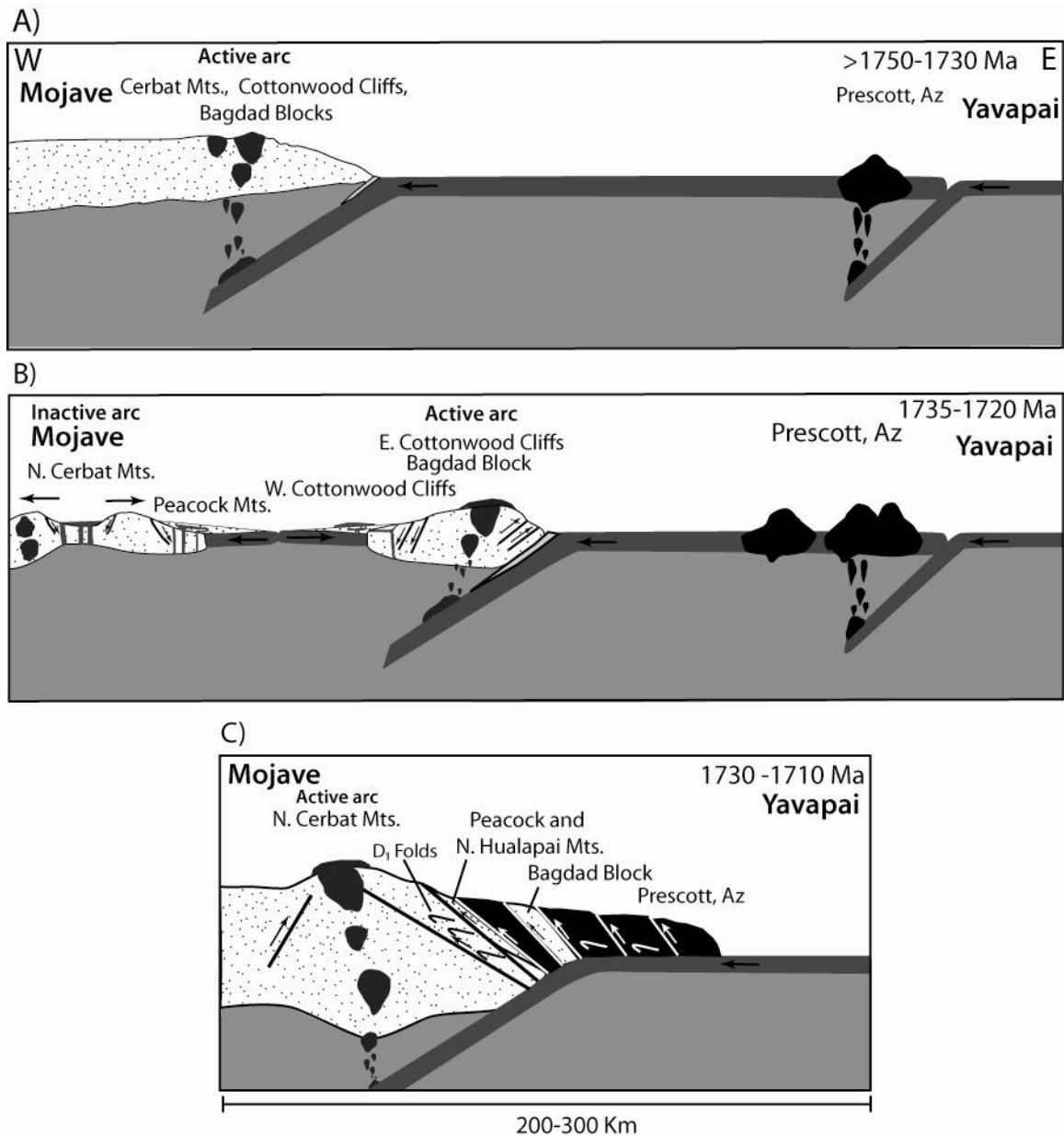


Figure 5-2: preliminary tectonic model for pre- to syn-D<sub>1</sub> back-arc rifting in the Mojave province. A) Proposed configuration of elements prior to formation of the boundary zone. With two west-northwest dipping subduction zones and associated volcanic arcs. B) Pre- to Syn-D<sub>1</sub> rifting of the Mojave Province (gray dots) and deposition of sediments along that margin. As well as back-arc spreading and deposition of volcanoclastic sedimentation C) D<sub>1</sub> collision of Mojave and Yavapai (black) provinces. Here this collision is modeled as successive accretion of island arcs and marginal basins rather than a collision of a continent or large terrane.

## Chapter 6

### Conclusions

#### Conclusions

- The Peacock Mountains record two deformational events;  $D_1$  and  $D_2$ , which are similar to fabrics identified in the northern Hualapai Mountains (Siwiec, 2003). Siwiec (2003) argued that the local  $D_2$  deformation is an intermediate deformational event in between regional  $D_1$  and  $D_2$  events. However, based on geochronology of syndeformational zircon and sphene from the Peacock Mountains (1.68 Ga) (Albin et al., 1991), I attribute  $D_2$  in the Peacock Mountains to the regional  $D_2$  deformation.
- Mineral assemblages and quantitative metamorphic temperature and pressure determinations of  $\sim 600^\circ\text{C}$  and 5.4 kbars are broadly consistent with regional granulite facies metamorphism in the Mojave province.
- Abundant quartz-rich metasedimentary and intermediate to mafic metavolcanic rocks in the Peacock Mountains are consistent with extensional back-arc sedimentation and arc volcanism (Packer and Ingersoll, 1986; Marsaglia et al., 1992; Marsaglia, 1995).
- Based on interpretations of depositional environment of metasedimentary and metavolcanic rocks in the Peacock Mountains and similar metasedimentary rocks in the northern Hualapai Mountains and Cottonwood Cliffs (Evans, 1999; Siwiec, 2003), I propose an extensional back-arc rifting model for the sedimentation and volcanism. This model is

also permissible in the context of existing data on syn-D<sub>1</sub> plutonic and metavolcanic rocks identified in nearby ranges (Chamberlain and Bowring, 1990; Duebendorfer et al., 2001; Bryant et al., 2001; Wooden and DeWitt, 1991).

## References

- Albin, A.L., and Karlstrom, K.E., 1991, Orthogonal Proterozoic fabrics in northwestern Arizona: Multiple orogenic events of progressive deformation during continental assembly, *in* Karlstrom, K.E., ed., Proterozoic geology and ore deposits of Arizona: Arizona Geological Society Digest, v. 19, p. 67-84.
- Albin, A.L., Shastri, L.L., Bowring, S.A., Karlstrom, K.E., 1991, Geologic and geochronologic data from the Gneiss Canyon shear zone of NW Arizona: timing and development of orthogonal fabrics: Geological Society of America Abstracts with Programs, v. 23, p. 1.
- Anderson, C.A., and Silver, L.T., 1976, Yavapai Series, a greenstone belt: Arizona Geological Society Digest, v. 10, p. 13-26.
- Anderson, C.A., Blacet, P.M., Silver, L.T., and Stern, T.W., 1971, Revision of the Precambrian stratigraphy in the Prescott-Jerome area, Yavapai County, Arizona: U.S. Geological Survey Bulletin, Report, B 1324-C, p.C1-C16, 1971.
- Anderson, C.A., Wooden, J.L., and Bender, E.E., 1993, Mojave province of southern California and vicinity, *in* Van Schmus, W.R., et al., 1993, Transcontinental Proterozoic provinces, *in* Reed, J.C., Jr., et al., eds., Precambrian: Conterminous U.S.: Boulder, Colorado, Geological Society of America, Geology of North America, v. C-2, p. 176-188.
- Anderson, P., 1986a, The Proterozoic tectonic evolution of Arizona: Tucson, University of Arizona, Ph.D. dissertation, 416 p.

- Anderson, P., 1986b, Summary of the Proterozoic plate tectonic evolution of Arizona from 1900 to 1600 Ma, *in* Beatty, B., and Wilkinson, P.A.K., eds., *Frontiers in geology and ore deposits of Arizona and the Southwest: Tucson, Arizona Geological Society Digest*, v. 16, p. 5-11.
- Anderson, P., 1989, Proterozoic plate tectonics evolution of Arizona, *in* Jenney, J.P., and Reynolds, S.J., eds., *Geologic evolution of Arizona: Arizona Geological Society Digest*, v. 17, p. 17-56.
- Beard, L. S., Lucchitta, I., 1993, Geologic map of the Valentine Southeast quadrangle, Mohave County, Arizona: U.S. Geological Survey, Report 90-201, 1 sheet.
- Bennett, V.C., and DePaolo, D.J., 1987, Proterozoic crustal history of the western United States as determined by neodymium isotopic mapping: *Geologic Society of America Bulletin*, v. 99, p. 674 – 685.
- Bonamici, C., 2007, Anatexis and exhumation of a Paleoproterozoic orogen, southern Hualapai Mountains, Arizona [M.S. thesis]: Northern Arizona University, 207 p.
- Bickford, M.E., and Hill, B.M., 2007, Does the arc accretion model adequately explain the Paleoproterozoic evolution of southern Laurentia?: An expanded interpretation: *Geology*, v. 35, p. 167-170.
- Bryant, B., Wooden, J.L., Nealey, L.D., 2001, *Geology, Geochronology, Geochemistry, and Pb-Isotopic Compositions of Proterozoic Rocks, Poachie Region, West-Central Arizona—A Study of the East Boundary of the Proterozoic Mojave Crustal Province*: U.S. Geological Survey Professional Paper 1639, 62 p.
- Chamberlain, K.R., and Bowring, S.A., 1990, Proterozoic geochronology and isotopic boundary in NW Arizona: *Geology*, v. 98, p. 399-416.

- Coleman, D.S., Barth, A.P., and Wooden, J.L., 2000, Early to Middle Proterozoic construction of the Mojave Province, southwestern United States: *Gondwana Research*, v. 5, p. 75-78.
- Collins, W.J., 2002, Hot orogens, tectonic switching, and creation of continental crust: *Geology*, v. 30, p. 535-538.
- Condie, K.C., 1982, Plate tectonics models for Proterozoic continental accretion in the southwestern United States: *Geology*, v. 10, p. 37-42.
- Condie, K.C., Lee, D., and Farmer, G.L., 2001, Tectonic setting and provenance of the Neoproterozoic Uinta Mountain and Big Cottonwood groups, northern Utah: constraints from geochronology, Nd isotopes, and detrital modes: *Sedimentary Geology*, v. 141-141, p. 443-464.
- Cox, R., Martin, M.W., Comstock, J.C., Dickerson, L.S., Ekstrom, I.L., and Sammons, J.H., 2002, Sedimentology, stratigraphy, and geochronology of the Proterozoic Mazatzal Group, central Arizona: *Geological Society of America Bulletin*, v. 114, no. 4, p. 1535-1549.
- Dickinson, W.R., Beard, L.S., Brakenridge, G.R., Erjavec, J.L., Ferguson, R.C., Inman, K.F., Knepp, R.A., Lindberg, F.A., Ryberg, P.T., 1983, Provenance of North American Phanerozoic sandstones in relation to tectonic setting: *Geological Society of America Bulletin*, v. 94, p. 222-235.
- Duebendorfer, E.M., Chamberlain, K.R., and Jones, C.S., 2001, Paleoproterozoic tectonic history of the Mojave-Yavapai boundary zone: Perspective from the Cerbat Mountains, northwestern Arizona: *Geological Society of America Bulletin*, v. 113, p. 575-590.

- Duebendorfer, E.M., Chamberlain, K.B, and Fry, B., 2006, Mojave-Yavapai boundary zone southwestern United States: A rifting model for the formation of an isotopically mixed crustal boundary zone: *Geology*, v. 34, p. 681-684.
- Dumond, G., Mahan, K.H., Williams, M.L., and Karlstrom, K.E., 2007, Crustal segmentation, composite looping pressure-temperature paths, and magma-enhanced metamorphic field gradients: Upper Granite Gorge, Grand Canyon, USA: *Geological Society of America Bulletin*, v. 119, p. 202-220.
- Evans, P.J., 1999, Proterozoic structure and geology of the Cottonwood Cliffs, Mohave County, Arizona [M.S. thesis]: Flagstaff, Northern Arizona University, 176 p.
- Faulds, J.E., Schreiber, B.C., Reynolds, S.J., González, L.A., Okaya, D., 1997, Orogen and Paleogeography of an immense, nonmarine Miocene salt deposit in the Basin and Range (western USA): *Journal of Geology*, v. 105, p. 19-36
- Ferguson, C.B., 2002, Deformation associated with the 1.4 Ga Borianna Canyon pluton, Northwestern Arizona: Regional strain or magma emplacement: [M.S. thesis]: Flagstaff, Northern Arizona University, 113 p.
- Hamilton, W., 1979, Tectonics of the Indonesian Region: U.S. Geological Survey Professional paper, 1078.
- Hawkins, D.P., Bowring, S.A., Ilg, B.R., Karlstrom, K.E., and Williams, M.L., 1996, U-Pb geochronologic constraints on the Paleoproterozoic crustal evolution of the Upper Granite Gorge, Grand Canyon, Arizona: *Geological Society of America Bulletin*, v. 108, p. 1167-1181.

- Holdaway, M.J., 2001, Recalibration of the GASP geobarometer in light of recent garnet and plagioclase activity models and versions of the garnet-biotite geothermometer: *American Mineralogist*, v. 86, p. 1117-1129.
- Holdaway, M.J., 2000, Application of new experimental garnet Margulas data to the garnet-biotite geothermometer: *American Mineralogist*, v. 85, p. 881-892.
- Howard, K.A., Intrusion of horizontal dikes: Tectonic significance of middle Proterozoic diabase sheets widespread in the upper crust of the southwestern United States: *Journal of Geophysical research*, v. 96, p. 12,461-12,478.
- Hill, B.M., and Bickford, M.E., 2001, Paleoproterozoic rocks of central Colorado: accreted arcs or extended older crust?: *Geology*, v. 29, p. 1015-1018.
- Ilg, B.R., Karlstrom, K.E., Hawkins, D.P., and Williams, M.L., 1996, Tectonic evolution of Paleoproterozoic rocks in the Grand Canyon: Insight into middle-crustal processes: *Geological Society of America Bulletin*, v. 108, p. 1149-1166.
- Iriondo, A., Premo, W.R., Martínez-Torres, L.M., Atkinson, W.W., Siems, D.F., Guarás-González, B., 2004, Isotopic, geochemical, and temporal characterization of Proterozoic basement rocks in the Quitovac region, northwestern Sonora, Mexico: Implications for the reconstruction of the southwestern margin of Laurentia: *Geological Society of America Bulletin*, v. 116, p. 154-170.
- James, S.C., Duebendorfer, E.M., and Hoisch, T.D., 2001, Location of the granulite-amphibolite facies transition in northwestern Arizona: *Geological Society of America Abstracts with Programs*, v. 33, p. 24.

- Jessup, M.J., Karlstrom, K.E., Connelly, J., Williams, M., Livaccari, R., Tyson, A., and Rodgers, S., 2005, Complex Proterozoic crustal assembly of southwestern North America in an arcuate subduction system: the Black Canyon of the Gunnison, Southwestern Colorado, *in* Karlstrom, K.E., and Keller, E., *The Rocky Mountain region: an evolving lithosphere*, geophysical monograph series, v. 154, p. 21-38.
- Jones, C.S., Duebendorfer, E.M., and Hoisch, T.D., 1998, Structure and metamorphism of the Vock Canyon area, Cerbat Mountains, Arizona: Implications for amalgamation and accretion of the Mojave and Yavapai Proterozoic crustal provinces: *Geological Society of America Abstracts with Programs*, v. 30, no. 6, p. 12.
- Jones, J.V., Connelly, J.N., Karlstrom, K.E., Williams, M.L., and Doe, M.F., 2009, Age, provenance, and tectonic setting of Paleoproterozoic quartzite successions in the southwestern United States: *Geological Society of America Bulletin*, v. 121, p. 247-264.
- Karlstrom, K.E., and Bowring, S.A., 1988, Early Proterozoic assembly of tectonostratigraphic terranes in southwestern North America: *Journal of Geology*, v. 96, p. 561-576.
- Karlstrom, K.E., and Bowring, S.A., 1993, Proterozoic orogenic history of Arizona, *in* Van Schmus et al., 1993, *Transcontinental Proterozoic provinces*, *in* Reed, J.C., jr., et al., eds., *Precambrian: Conterminous U.S.: Boulder Colorado*, Geological Society of America, *Geology of North America*, v. C-2, p. 188-211.

- Karlstrom, K.E., and Humphreys, G., 1998, Influence of Proterozoic accretionary boundaries in the tectonic evolution of western North America: Interaction of cratonic grain and mantle modification events: *Rocky Mountain Geology*, v. 33, p. 161–179.
- Kleemann, U., and Reinhardt, J., 1994, Garnet-biotite thermometer revisited: The affect of  $Al^{vi}$  and Ti in biotite: *European Journal of Mineralogy*, v. 6, p. 925-941.
- Koziol, A.M., and Newton, R.C., 1988, Redetermination of the anorthite breakdown reaction and improvement of the plagioclase-garnet- $Al_2SiO_5$ -quartz geothermobarometer: *American Mineralogist*, v. 73, p. 216-223.
- Lister, G., and Forster, M., 2009, Tectonic mode switching and the nature of orogenesis: *Lithos*, v. ? (in press).
- Low, P.C., Seaman, S.J., Karlstrom, K.E., and Williams, M.L., 2002, Proterozoic ultramafic rocks in southwestern North America; distinguishing ophiolites from arc cumulates: *Geological Society of America Abstracts with Programs*, v. 34, p. 181.
- Low, P.C., Seaman, S.J., Jerciovic, M.J., Williams, M.L., Geochemical evidence for pulse magma and fluid interaction in the Mile 91 Peridotite, Grand Canyon, USA; implications for interpretation of Proterozoic tectonic setting: *Geological Society of America Abstracts with Programs*, v. 35, p. 321.
- Marsaglia, K.M., 1995, Interarc and Backarc Basins, *in* Busby, C.J. and Ingersol, R.V., eds., *Tectonics of sedimentary basins*: Cambridge, Blackwell Science, p. 399-330.

- Marsaglia, K.M., Ingersoll, R.V., Packer, B.M., 1992, Tectonic evolution of the Japanese islands as reflected in modal compositions of Cenozoic forearc and backarc sand and sandstone: *Tectonics*, v. 11, p. 1266-1287.
- Packer, B.M., and Ingersoll, R.V., 1986, Provenance and petrology of Deep Sea Drilling Project sands and sandstones from the Japan and Mariana forearc and backarc regions: *Sedimentary Geology*, v. 51, p. 5-28.
- S.M. Richard, S.J. Reynolds, J.E. Spencer, and P.A. Pearthree, compilers, 2000, Geologic map of Arizona, Arizona Geological Survey Map M35, 1:1,000,000 scale. Revision of original 1988 map (AGS Map 26).
- Robinson, K., 1994, Metamorphic petrology of the lower Granite Gorge and the significance of the Gneiss Canyon shear zone, Grand Canyon, Arizona [M.S. thesis]: Amherst, University of Massachusetts, 187 p.
- Patiño-Douce, A.E., and Johnston, A.D., 1991, Phase equilibria and melt productivity in the pelitic system; implications for the origin of peraluminous granitoids and aluminous granulites: *Contributions to Mineralogy and Petrology*, v. 107, p. 202-218.
- Shastri, L.L., Chamberlain, K.R., and Bowering, S.A., 1991, Inherited zircon from ca. 1.1 Ma mafic dikes, NW Arizona: *Geological Society of America Abstracts with Programs*, v. 23, no. 4, p. 93.
- Siwiec, B.R., 2003, Tectonic implications of Paleoproterozoic structure and metamorphism in the northern Hualapai Mountains, Mohave county, Arizona [M.S. thesis]: Northern Arizona University, 103 p.

- Spear, F.S., 1981, An experimental study of hornblende stability and compositional variability in amphibolite: *American Journal of Science*, v. 281, p. 697-734.
- Spear, F.S., Kohn, M.J., Cheney, J.T., 1999, P-T paths from anatexis in pelites: *Contributions to Mineral Petrology*, v. 137, p. 17-32.
- Van Schmus, W.R., Bickford, M.E., and Turek, E., 1996, Proterozoic geology of the east-central mid-continent basement, *in* van der Pluijm, B.A., and Catacosinos, P.A., eds., *Basement and basins of eastern North America: Geological Society of America Special Paper 308*, p. 7–32.
- Thompson, A.B., Connolly, J.A.D., 1995, Melting of the continental crust: some thermal and petrological constraints on anatexis in continental collision zones and other tectonic settings: *Journal of Geophysical Research*, v. 100, p. 15565-15579.
- Thompson, J.B. Jr., Thompson, A.B., 1976, A model system for mineral facies in pelitic rocks: *Contributions to Mineral Petrology*, v. 58, p. 243-277.
- Thy, P., 1992, Petrology of basaltic sills from Ocean Drilling Program sites 794 and 797 in the Yamato Basin of the Japan Sea: *Journal of Geophysical Research*, v. 11, p. 9027-9042.
- Todd, C.S., 1998, Limits on the precision of geobarometry at low grossular and anorthite content: *American Mineralogist*, v. 83, p. 1161-1167.
- Whitmeyer, S.J., and Karlstrom, K.E., 2007, Tectonic model for Proterozoic growth of North America: *Geosphere*, v. 3, p. 220-258.
- Windley, B.F., 1993, Proterozoic anorogenic magmatism and its orogenic connection: *Geological Society [London] Journal*, v. 150, p. 39–50.

- Wooden, J.L., and Aleinikoff, J.N., 1987, Pb isotopic evidence for Early Proterozoic crustal evolution in the southwestern U.S.: Geological Society of America Abstracts with Programs, v. 19, p. 897.
- Wooden, J.L., and DeWitt, E., 1991, Pb isotopic evidence for a major early crustal boundary in western Arizona, *in* Karlstrom, K.E., ed., Proterozoic geology and ore deposits of Arizona: Arizona Geological Digest 19, p. 27 – 50.
- Wooden, J.L., and Miller, D.M., 1990, Chronologic and isotopic framework for Early Proterozoic crustal evolution in the eastern Mojave desert region, California: Journal of Geophysical Research, v. 95, p. 20,133-20,146.
- Wooden, J.L., Nutman, A.P., Miller, D.M., Howard, K.A., Bryant, B., DeWitt, E., and Mueller, P.A., 1994, SHRIMP U-Pb zircon evidence for late Archean and early Proterozoic crustal evolution in the Mojave and Arizona crustal provinces: Geological Society of America Abstracts with Programs, v. 26, no. 6, p. 69.
- Wooden, J.L., Stacey, J.S., Doe, B., Howard, K.A., and Miller, D.M., 1988, Pb isotopic evidence for the formation of Proterozoic crust in the southwestern United States, *in* Ernst, W.G., ed., Metamorphism and Crustal evolution of the Western United States: Englewood Cliffs, New Jersey, Prentice Hall, Rubey Volume VII, p. 68–86.
- Zorin, Y.A., Sklyarov, E.V., Belichenko, V.G., Mazukabzov, A.M., 2009, Island arc–back-arc basin evolution: implications for Late Riphean–Early Paleozoic geodynamic history of the Sayan–Baikal folded area: Russian Geology and Geophysics, v. 50, p. 149–161.

## Appendix A

### Mineral Assemblages

Mineral	Abbreviation	Mineral	Abbreviation
Hornblende	Hbl	k-feldspar	k-spar
Quartz	Qtz	Garnet	gar
Sillimanite	Sil	Muscovite	mus
Clinopyroxene	Cpx	Chlorite	chl
Olivine	ol	Zircon	zr
Amphibole	amp	opaques	op
Spinel	sp	Sphene	Sph
Epidote	ep	Apatite	ap

Sample	Location	Map Unit	Rock type	Qtz	Sil	amp	Hbl	Pl	K-spar	Bio	Gar	ap	Mus	ep	Sp	Zr	ol	Sph	Chl	opx	Cpx	op	
MP 3/18/08-1	12N 0248370, 3906000	Xms	Psammitic schist	x			x	x	x	x	x		x									x	
MP 5/12/08-1	12N 0248506, 3905486	Xms	Psammitic schist	x				x	x	x	x												
MP 5/13/08-1	12N 0248364, 3907013	Xms	Psammitic schist	x				x	x	x	x												
MP 5/13/08-2	12N 0248388, 3907203	Xms	Psammitic schist	x			x	x	x	x													
MP 5/25/08-2	12N 0248487, 3906847	Xms	Psammitic schist	x				x	x	x													

MP 5/25/08-4	MP 5/14/08-3	MP 5/14/08-2	MP 5/14/08-1	MP 1/6/09-3	MP 1/6/09-2	MP 12/13/08-3	MP 5/26/08-6	Sample
12N 0248393, 3906497	12N 0249171, 3905009	12N 0249171, 3905009	12N 0249188, 3905022	12N 0249563, 3906672	12N 0248922, 3907453	12N 0248656, 3903980	12N 0250234, 3906286	Location
Xms	Map Unit							
Pelitic schist	Pelitic schist	Pelitic schist	Pelitic schist	Psammitic schist	Psammitic schist	Psammitic schist	Psammitic schist	Rock type
x	x	x	x	x	x	x	x	Qtz
x	x	x	x					Sil
								amp
					x			Hbl
x	x		x	x	x	x	x	Pl
x	x	x	x	x	x	x		K-spar
x	x	x	x	x	x	x	x	Bio
x	x	x	x					Gar
								ap
								Mus
								ep
			x					Sp
					x		x	Zr
								ol
								Sph
								Chl
								opx
								Cpx
						x		op

MP 5/13/08-3	MP 12/12/08-2	MP 5/26/08-3	MP 3/18/08-2	MP 12/13/08-2	MP 12/13/08-1B	MP 5/26/08-5	MP 5/26/08-2	Sample
12N 0248394, 3907221	12N 0247909, 3907180	12N 0250163, 3906979	12N 0248392, 3907202	12N 0249628, 3904080	12N 0249651, 3904091	12N 0250483, 3907000	12N 0250313, 3906738	Location
Xms	Xmg	Xmg	Xmg	Xms	Xms	Xms	Xms	Map Unit
ultramafic	Mafic gneiss	Mafic gneiss	Mafic gneiss	Pelitic schist	Pelitic schist	Pelitic schist	Pelitic schist	Rock type
	x		x	x	x	x	x	Qtz
x								Sil
								amp
	x		x					Hbl
	x	x	x	x	x	x	x	Pl
	x							K-spar
x				x	x	x	x	Bio
				x	x		x	Gar
			x					ap
				x		x		Mus
	x		x					ep
								Sp
	x	x						Zr
x		x						ol
	x	x	x					Sph
								Chl
x								opx
	x							Cpx
x						x		op

MP 5/26/08-7	MP 5/26/08-1	MP 1/6/09-1	Sample	MP 5/25/08-3	Sample
unknown	12N 0250558, 3906622	12N 0249454, 3907351	Location	12N 0248401, 3906729	Location
	Ygr	Xms	Map Unit	Xms	Map Unit
diabase dike	granite	ultramafic	Rock type	ultramafic	Rock type
	x		Qtz		Qtz
			Sil		Sil
			amp	x	amp
x			Hbl		Hbl
x	x		Pl		Pl
	x		K-spar		K-spar
x	x		Bio	x	Bio
	x		Gar		Gar
			ap		ap
	x		Mus		Mus
			ep		ep
			Sp		Sp
			Zr	x	Zr
			ol	x	ol
			Sph		Sph
		x	Chl		Chl
		x	opx	x	opx
			Cpx		Cpx
	x		op		op

## Appendix B

### Electron Microprobe Analysis

Electron Mircoprobe Analysis of MP 5/14/08-3						
Biotites						
Analysis	bt 1	bt 1	bt 1	bt 2	bt 2	bt2
Na <sub>2</sub> O	0.099	0.11	0.079	0.094	0.099	0.079
MgO	6.55	6.6	6.657	6.296	6.614	6.837
Al <sub>2</sub> O <sub>3</sub>	20.24	20.406	19.981	20.063	19.858	19.71
SiO <sub>2</sub>	34.112	33.406	33.879	33.827	34.309	34.572
K <sub>2</sub> O	10.134	9.753	10.297	10.13	10.02	10.128
CaO	0	0.016	0	0	0.004	0
TiO <sub>2</sub>	1.601	1.538	1.517	1.704	1.663	1.664
MnO	0.138	0.133	0.136	0.166	0.173	0.146
FeO	23.945	22.676	22.787	23.068	23.096	22.437
Totals	96.82	95.163	95.242	95.348	95.837	95.574
Na	0.073	0.081	0.058	0.069	0.074	0.059
Mg	3.95	3.98	4.014	3.797	3.988	4.123
Al	10.713	10.8	10.527	10.619	10.51	10.432
Si	15.946	15.861	15.837	15.812	16.038	16.16
K	8.413	8.097	8.548	8.41	8.318	8.407
Ca	0	0.011	0	0	0.003	0
Ti	0.96	0.966	0.909	1.022	0.997	0.997
Mn	0.107	0.103	0.105	0.129	0.134	0.133
Fe 2+	18.613	17.626	17.713	17.931	17.953	17.441
Garnets						
Garnet A						
Analysis	GA 1	GA 2	GA 3			
Na <sub>2</sub> O	0	0	0			
MgO	1.696	1.67	1.725			
Al <sub>2</sub> O <sub>3</sub>	21.208	21.458	21.151			
SiO <sub>2</sub>	36.234	36.765	36.386			
K <sub>2</sub> O	0.017	0.013	0.02			
CaO	1.326	1.323	1.365			
TiO <sub>2</sub>	0.05	0.035	0.031			
MnO	4.423	4.452	4.679			

FeO	35.575	35.157	35.45			
Totals	100.528	100.873	100.806			
Na	0	0	0			
Mg	1.023	1.007	1.04			
Al	11.224	11.357	11.195			
Si	16.938	17.186	17.009			
K	0.014	0.011	0.016			
Ca	0.947	0.946	0.975			
Ti	0.03	0.021	0.018			
Mn	3.425	3.448	3.624			
Fe 2+	27.653	27.328	27.556			
Garnet B						
Analysis	GB 1	GB 2	GB 3	GB 4		
Na <sub>2</sub> O	0.007	0.003	0	0		
MgO	1.566	1.743	1.762	1.737		
Al <sub>2</sub> O <sub>3</sub>	21.575	21.262	21.528	21.243		
SiO <sub>2</sub>	36.766	36.995	36.829	36.489		
K <sub>2</sub> O	0.02	0.006	0.014	0.017		
CaO	1.366	1.303	1.326	1.334		
TiO <sub>2</sub>	0.049	0.037	0.048	0.028		
MnO	4.318	4.053	4.741	4.592		
FeO	35.573	35.265	35.381	35.422		
Totals	101.241	100.666	101.631	100.861		
Na	0.005	0.003	0	0		
Mg	0.944	1.051	1.063	1.047		
Al	11.419	11.253	11.394	11.242		
Si	17.186	17.293	17.216	17.056		
K	0.017	0.005	0.012	0.014		
Ca	0.977	0.931	0.948	0.953		
Ti	0.029	0.022	0.029	0.017		
Mn	3.344	3.139	3.672	3.556		
Fe 2+	27.651	27.412	27.502	27.534		
Plagioclase						
Analysis	P 1	P 1				

Na <sub>2</sub> O	8.111	9.175				
MgO	0	0				
Al <sub>2</sub> O <sub>3</sub>	24.616	23.814				
SiO <sub>2</sub>	63.721	63.976				
K <sub>2</sub> O	0.097	0.099				
CaO	5.306	4.643				
TiO <sub>2</sub>	0	0				
MnO	0.007	0.034				
FeO	0	0				
Totals	101.858	101.741				
Na	6.017	6.807				
Mg	0	0				
Al	13.028	12.604				
Si	29.786	29.905				
K	0.081	0.082				
Ca	3.792	3.318				
Ti	0	0				
Mn	0.005	0.026				
Fe 2+	0	0				

## **Biographical Information**

**Name of Author:** Mitchell Ryan Prante

**Place of Birth:** San Diego, California, USA.

**Date of Birth:** October 21, 1986

### **Educational Degrees Awarded**

University of California at Santa Barbara, B.S., 2007.

Northern Arizona University, M.S., 2009.

### **Scholarly Publications**

Prante, M.R., and Duebendorfer, E.M., 2009, Paleoproterozoic deformation and metamorphism in the central and southern Peacock Mountains, NW Arizona:

Implications for the location of the Mojave-Yavapai boundary zone: Geological

Society of America Abstracts and Programs, v. 41, No. 6, p. 37.

Prante, M.R., and Duebendorfer, E.M., Paleoproterozoic deformation and metamorphism

in the central and southern Peacock Mountains, NW Arizona: Implications for

tectonic setting of the Mojave-Yavapai boundary zone (*in progress*)